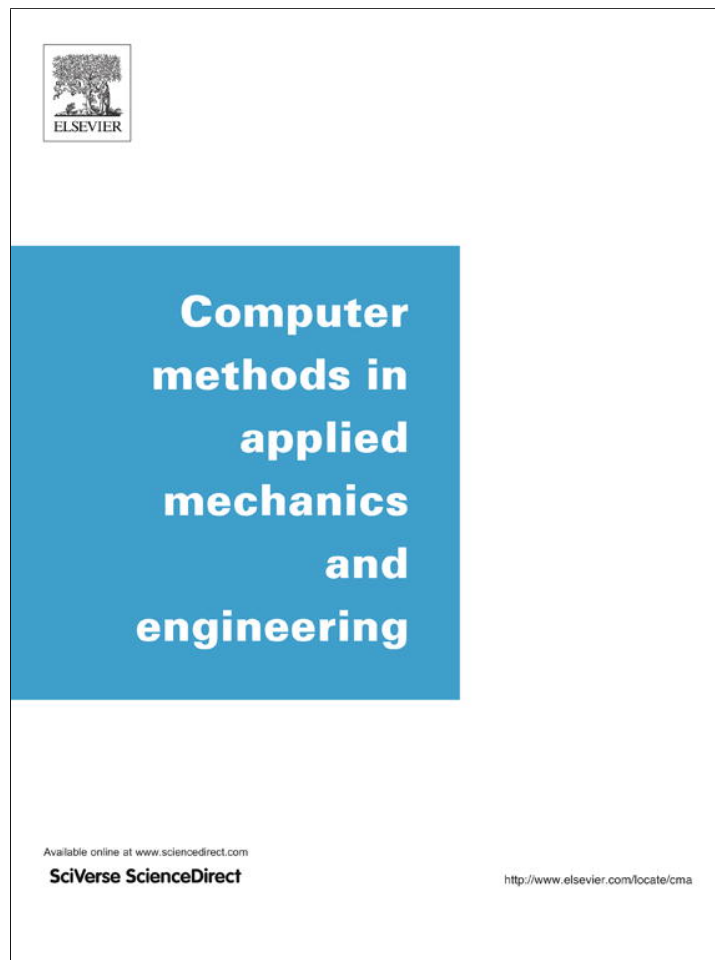


Provided for non-commercial research and education use.
Not for reproduction, distribution or commercial use.



(This is a sample cover image for this issue. The actual cover is not yet available at this time.)

This article appeared in a journal published by Elsevier. The attached copy is furnished to the author for internal non-commercial research and education use, including for instruction at the authors institution and sharing with colleagues.

Other uses, including reproduction and distribution, or selling or licensing copies, or posting to personal, institutional or third party websites are prohibited.

In most cases authors are permitted to post their version of the article (e.g. in Word or Tex form) to their personal website or institutional repository. Authors requiring further information regarding Elsevier's archiving and manuscript policies are encouraged to visit:

<http://www.elsevier.com/copyright>



Contents lists available at SciVerse ScienceDirect

Comput. Methods Appl. Mech. Engrg.

journal homepage: www.elsevier.com/locate/cma

Projected event-capturing time-stepping schemes for nonsmooth mechanical systems with unilateral contact and Coulomb's friction



Vincent Acary

INRIA, Grenoble Rhône-Alpes, BIPOP Team-Project, 655, Avenue de l'Europe, 38334 Saint Ismier, Cedex, France

ARTICLE INFO

Article history:

Received 8 August 2012

Received in revised form 10 December 2012

Accepted 23 December 2012

Available online 7 January 2013

Keywords:

Computational contact mechanics

Flexible multibody dynamics

Unilateral contact

Impact

Coulomb's friction

Gear–Gupta–Leimkuhler (GGL) technique

ABSTRACT

This work addresses the problem of the numerical time-integration of nonsmooth mechanical systems subjected to unilateral contacts, impacts and Coulomb's friction. The considered systems are the space-discretized continuous systems obtained by using a Finite Element Method (FEM) approach or the multi-body systems, or a mix of them as in flexible multibody dynamics. Up to now, two main numerical schemes are available for this purpose: the Moreau–Jean scheme which solves the constraints at the velocity level together with a Newton impact law and the Schatzman–Paoli scheme which directly considers the constraints at the position level. In both schemes, the position and velocity constraints are not both satisfied in discrete time. A first attempt to improve the time simulation is made by directly using the Gear–Gupta–Leimkuhler (GGL) approach for Differential Algebraic Equations (DAE), that solves, in discrete time, the constraints on both position and velocity levels. This obtained direct projection scheme succeeds in solving in discrete time both position and velocity constraints, but introduces some chattering at contact after a finite accumulation of impacts. A second new scheme is proposed that improves the direct projected scheme by combining several steps of activation and projection to avoid the chattering effect. The stability and the local order of the scheme will be discussed. The usefulness of the scheme is demonstrated on several academic examples and is illustrated on an industrial application: the modeling and simulation of an electrical circuit breaker.

© 2012 Elsevier B.V. All rights reserved.

1. Introduction and motivations

This work addresses the problem of the numerical time-integration of nonsmooth mechanical systems subjected to unilateral contacts, impacts and Coulomb's friction. The targeted systems are the multi-body systems where interconnected rigid or flexible bodies interact through perfect joints and ideal unilateral frictional interfaces. As flexibility may have an important role in the global dynamical behavior, we are also interested in considering discrete systems which result of a space-discretization of a solid, for instance, by finite element techniques.

The simulation, and especially time-integration of nonsmooth mechanical systems with unilateral contacts is an active research domain due to the complexity of performing an efficient, accurate and robust simulation. The main issue is the inherent nonsmoothness of the time evolution as a result of the nonsmoothness of the models based on the unilateral contact (Signorini's condition) and Coulomb's friction. It is well-known that the presence of unilateral contact may imply the occurrence of impacts (velocity jumps and/or reaction impulses) and Coulomb's friction may also generate velocity jumps as in the well-known Painlevé example [19]. This

demand for specific time-integration techniques which are usually classified into two categories: the *event-tracking time-stepping schemes* (also commonly and shortly called event-driven schemes) and the *event-capturing time-stepping schemes* (shortly time-stepping schemes). The first family of schemes is based on an accurate detection of events (closing and opening contacts, changes in the direction of sliding, transition from sliding to sticking or vice-versa, ...). Such schemes are mainly dedicated to systems with a small number of events and mainly in the two-dimensional configuration. For more details on such schemes, we refer to [42] and [4, Chapter 8].

When a large number of events are expected in three-dimensional configurations, only event-capturing time-stepping schemes are sufficiently efficient and robust. This is the case for structural dynamics, and multibody dynamics where the density of events with respect to time prevents the use of an accurate detection of the instants of events. Two main numerical schemes available to integrate the nonsmooth dynamics with impacts: the Moreau–Jean scheme [35,27,36,26] which solves the constraints at the velocity level together with a Newton impact law and the Schatzman–Paoli scheme [49,39,40] which directly considers the constraints at the position level. For these schemes, rigorous mathematical analysis have been carried out [34,52,16] and numerous large scale

E-mail address: vincent.acary@inria.fr

applications have proven their own interests [44]. These schemes have also numerous variants that have been presented in the literature (see [4] for details), but in any of these schemes, the position and velocity constraints are both satisfied in discrete time.

In computational contact mechanics of solids and structures, the Newmark family of schemes (HHT, α -scheme, ...) are generally used for the time integration of space-discretized structures with Signorini's condition and Coulomb's friction [56,58,14,15]. In these latter approaches, it is implicitly assumed that the solutions (position/displacements, velocities, contact forces) are sufficiently smooth such that the Newmark family of second-order schemes can be applied without problems. In our case, the contact activation between finite-freedom mechanical models induces the non-smoothness of the solutions. Therefore, the direct application of higher order schemes in this context may be hazardous. Some attempts have recently been made to improve the global order of accuracy of time-stepping with nonsmooth events [55,3,50].

The motivations to build a scheme satisfying constraints both at the position level and at the velocity level in discrete time are:

- The study of multi-body systems with clearances in joints. If the joints with clearances are modeled with unilateral contact, we need to keep the drift of the constraints as smallest as possible with respect to the characteristic lengths of the clearances.
- For multibody systems with perfect ideal joints (bilateral constraints), we want to be able to solve the well-known drift issue of the constraints if they are treated at the acceleration level or at the velocity level.
- In quasi-static applications, mostly when the finite element method is involved, we want to avoid penetration between bodies, so we want to enforce the constraint at the position level, but a smooth evolution of the local relative velocities at contact. Spurious oscillations at contact of the local velocities are an extensively studied issue in the literature [32,14]. Mimicking the plastic impact law at the velocity level (quasi-collision) allows one to stabilize the velocity and then the stresses at contact.
- Finally, the last motivation is to maintain the consistency of the geometrical model required by the computational geometry system of Computer Aided Design (CAD) tools. For most of collision detection algorithms, avoiding interpenetrations between bodies is a requirement to guarantee the efficiency and robustness of the results of the contact detection process.

The aim of this work is to propose a new strategy based on the Moreau–Jean time-stepping scheme which enforces in discrete time the constraints on both position and velocity levels. The quest for such a scheme is connected to the approaches of geometric numerical integration theory of differential systems where the discrete approximation of the solution preserves some geometrical properties of the flow [22]. In our case, we want that the solution preserves the constraints and the impact law in discrete time.

A first solution is proposed in Section 4 which makes a direct use of the Gear–Gupta–Leimkuhler (GGL) approach. The GGL technique for Differential Algebraic Equations (DAE) [18] solves, in discrete time, the constraints on both position and velocity levels. For this purpose, the authors introduced in the continuous time formulation, new kind of multipliers to enforce additional and redundant constraints and reducing by the way the index of the DAE. These multipliers can be understood as the multipliers associated with the projection onto the constraints. The direct application of this idea which was already suggested in [2,54] results in a scheme able to satisfy the constraints requirements in a very efficient way in most of the configurations. Results on the local order of the scheme are given and qualitative properties are discussed on several academic examples. Its main drawback lies in the introduction of numerical spurious oscillations when a contact is kept closed after

a finite accumulation of impacts. These spurious oscillations, termed as chattering in this paper, are mainly due to an harmful interaction between the unilateral condition and the increase of energy due to the projection onto constraints.

In Section 5, a new solution is proposed to circumvent the chattering problem. This solution improves the direct projected algorithm by using a special combination of the activation of the constraints at the velocity level and the projection onto these activated constraints. The new combined scheme is mainly based on the direct projected scheme and shares the same favorable properties (respect of the constraints, order, straightforward implementation). Furthermore, it cancels the chattering at contact and avoids increasing energy due to the projection.

The outline of the article is as follows. In Section 2, basic concepts and equations used to model nonsmooth multi-body systems are introduced. In Section 3, the basic time-stepping schemes *i.e.*, the Moreau–Jean scheme and the Schatzman–Paoli scheme are briefly reviewed. The direct application of the GGL idea is developed in Section 4. After the formulation of the scheme, some results on the local order of consistency are provided. The main drawback, the so-called chattering effect, is also exhibited on academic examples. A combined activation/projection procedure is investigated in Section 5, which gives a correct answer to our problem. Finally, applications are developed in Section 6 and we show on the slider–crank mechanism and on a model of a circuit breaker that the approach is a promising solution in industrial prototyping process of mechanisms with clearances. Section 7 concludes the article.

Notation. The following notation is used throughout the paper. The uniform norm for a function f is denoted by $\|f\|_\infty$ and for a vector $x \in \mathbb{R}^n$ by $\|x\|$. A function f is said to be of class C^p if it is continuously differentiable up to the order p . Let I denote a real time interval of any sort. The set of functions $f : I \rightarrow \mathbb{R}^n$ of bounded variations (BV) is denoted by $BV(I, \mathbb{R}^n)$. The set of functions $f : I \rightarrow \mathbb{R}^n$ of locally bounded variations (LBV) is denoted by $LBV(I, \mathbb{R}^n)$. For $f \in BV(I, \mathbb{R}^n)$, we denote the right-limit function by $f^+(t) = \lim_{s \rightarrow t, s > t} f(s)$, and respectively the left-limit by $f^-(t) = \lim_{s \rightarrow t, s < t} f(s)$. The value $\text{var}(f, I)$ denotes its total variation on I . We denote by $0 = t_0 < t_1 < \dots < t_k < \dots < t_N = T$ a finite partition (or a subdivision) of the time interval $[0, T]$ ($T > 0$). For the sake of simplicity, the length of a time step is considered to be constant and is denoted by $h = t_{k+1} - t_k$. The value of a real function $x(t)$ at the time t_k , is approximated by x_k . In the same way, the notation $x_{k+\theta} = (1 - \theta)x_k + \theta x_{k+1}$ is used for $\theta \in [0, 1]$. The notation $\mathcal{O}(h)$ is to be understood as $h \rightarrow 0$. The notation dt defines the Lebesgue measure on \mathbb{R} . The notation $N_C(x)$ is used for the normal cone in the Convex Analysis sense to a convex set C at the point x [45]. The function $\text{prox}_M(C, x)$ returns the closest element of C to x in the metric defined by a definite positive matrix M . For any matrix $A \in \mathbb{R}^{n \times n}$ and a set of indices $\alpha \subset \{1, \dots, n\} \subset \mathbb{N}$, $A_{\alpha\alpha}$ denotes the submatrix composed of the rows and the columns indexed by the indices in α . The matrix $A_{\alpha\cdot}$ (respectively $A_{\cdot\alpha}$) stands for the matrix that collects all the rows (respectively the columns) indexed by α . The matrix $I_{n \times n}$ denotes the identity matrix of $\mathbb{R}^{n \times n}$.

2. Nonsmooth mechanical systems with unilateral contact

In this section, we give the basic ingredients for the modeling of multibody systems with unilateral constraints. For more details on the modeling of multibody systems with unilateral constraints, we refer to [4,42,35] and for the mathematical analysis, we refer to [46,34,53,7].

2.1. The frictionless case in a pure Lagrangian setting

Let us first consider a pure Lagrangian setting. The equations of motion of multibody systems with unilateral constraints are

$$\begin{cases} q(t_0) = q_0, \quad v(t_0) = v_0, & (1a) \\ \dot{q}(t) = v(t), & (1b) \\ M(q(t))\dot{v}(t) + F(t, q(t), v(t)) = G(t, q)\lambda(t), & (1c) \\ g^\alpha(t, q(t)) = 0, \quad \alpha \in \mathcal{E}, & (1d) \\ g^\alpha(t, q(t)) \geq 0, \quad \lambda^\alpha \geq 0, \quad \lambda^\alpha g^\alpha(t, q) = 0 \quad \alpha \in \mathcal{I}, & (1e) \end{cases}$$

where

- $q(t) \in \mathbb{R}^n$ is the generalized coordinates vector and $v(t) = \dot{q}(t)$ the associated generalized velocities vector,
- the initial conditions are $q_0 \in \mathbb{R}^n$ and $v_0 \in \mathbb{R}^n$,
- $M(q(t)) \in \mathbb{R}^{n \times n}$ is the inertia, $F(t, q(t), v(t)) \in \mathbb{R}^n$ the forces,
- the function $g(t, q(t)) \in \mathbb{R}^m$ defines the constraints in the dynamical system, and $G^\top(t, q(t)) = \nabla_q^\top g(t, q(t))$ is the Jacobian matrix of g with respect to q ,
- $\lambda \in \mathbb{R}^m$ is the Lagrange multiplier vector associated with the constraints, and
- the sets $\mathcal{E} \subset \mathbb{N}$ and $\mathcal{I} \subset \mathbb{N}$, respectively describe the set of bilateral constraints (joints) and unilateral constraints (contacts).

Remark 1. In the Newton/Euler formalism [20,21,9], the vector of parameters q usually contains the position of the center of mass x and a parametrization of the finite rotation θ which models the orientation of the body with respect to a spatial frame. The velocity is usually composed of the velocity of the center of mass \dot{x} and of an angular velocity Ω expressed for instance in the inertial frame. Therefore, the velocity is not the time-derivative of the parameter vector q , but generally related to q by means of an operator $T(q)$ such that

$$\dot{q}(t) = T^\top(q(t))v(t). \tag{2}$$

The equations of motion (1) can be extended to the Newton/Euler formalism by considering (2) rather than (1b) and by defining G as $G(t, q(t)) = \nabla_q g(t, q(t))T(q(t))$.

In the remaining of the article, we will consider only the Lagrangian setting to make the notation clearer.

Remark 2. After a space-discretization of continuum solids by a finite element approach, the generalized coordinates vector q usually contains the nodal displacements, and possibly the nodal rotations if any. Nevertheless, the generalized velocity is most of the time-derivative of the coordinates q .

For the sake of simplicity, we also restrict our presentation to holonomic perfect unilateral constraints, that is, we will consider in this paper that $\mathcal{E} = \emptyset$ and that the constraints are scleronomic constraints, i.e. $g(t, q(t)) = g(q(t))$. Applications in Section 6 will however show more general cases. The constitutive law for the perfect unilateral constraints is given by the Signorini condition

$$0 \leq g(q(t)) \perp \lambda(t) \geq 0, \tag{4}$$

where the inequalities involving vectors are understood to hold component-wise and the $x \perp y$ symbol means that $y^\top x = 0$. Let us define the following variables relative to the constraints, called *local variables*: the local velocity $U(t)$ and the (local) Lagrange multiplier $\lambda(t)$ which is associated with the generalized reaction forces $r(t)$ such that

$$U(t) = G^\top(q)v(t), \quad r(t) = G(q)\lambda(t). \tag{5}$$

For finite-freedom mechanical systems, an impact law must be added to close the system of equations. The most simple impact law will be considered in this work given by Newton's impact law

$$U^+(t) = -eU^-(t), \quad \text{if } g(q(t)) = 0, \tag{6}$$

where e is the coefficient of restitution.

Throughout the paper, several academic test examples are chosen to outline the properties of the considered numerical integration schemes.

Example 1 (The bouncing ball). This is the standard bouncing ball under gravity depicted in Fig. 1(a). The dynamics is constant with a forcing term equal to f together with a unilateral contact on the ground,

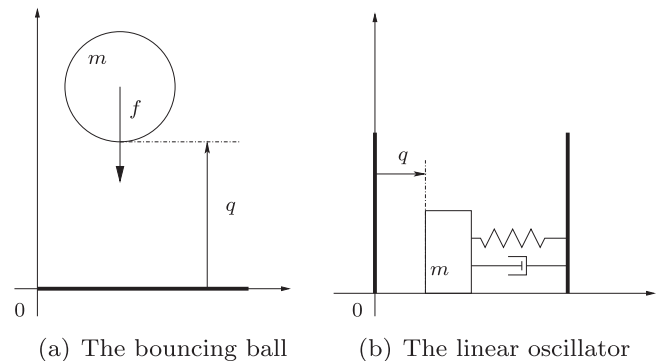
$$\begin{cases} \dot{v}(t) = f(t) + \lambda(t), & \dot{q}(t) = v(t), \\ 0 \leq q(t) \perp \lambda(t) \geq 0, & v^+(t) = -ev^-(t), \quad \text{if } q(t) = 0, \end{cases} \tag{7}$$

The interesting feature of the bouncing ball example is the presence of a finite accumulation of impact when $0 < e < 1$ and $f < 0$. The analytical solution of this example can be found in [10]. A more pleasant analytical solution due to Ballard [8] for $f = -2$ and $e = 1/2$ is detailed in [2]. It will be used as a benchmark in the further sections.

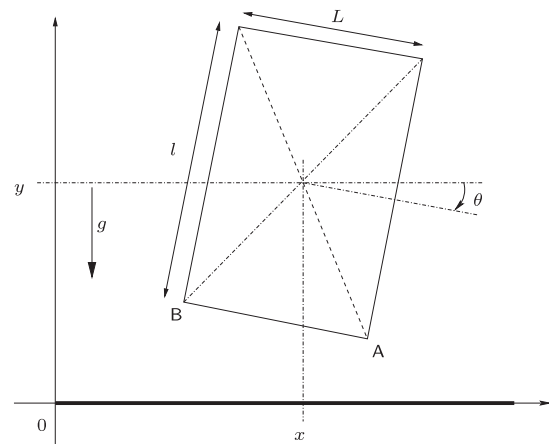
Example 2 (The linear oscillator). The dynamics of this one-degree-of-freedom system depicted in Fig. 1(b) example is similar to the bouncing ball dynamics in (7) but with a linear spring-damper internal force, that is

$$m\dot{v}(t) + cv(t) + kq(t) = \lambda(t). \tag{8}$$

The explicit analytical solution with impacts can be found in [25]. The previous trivial free dynamics (7) with a null or a constant forcing term are exactly integrated with any first order scheme. With the linear, but nontrivial, dynamical term in (8), the order of accuracy of higher order schemes can be exhibited.



(a) The bouncing ball (b) The linear oscillator



(c) The rocking block

Fig. 1. Simple archetypal test examples.

Example 3 (*The rocking block*). The rocking block of length L and thickness l is depicted in Fig. 1(c). Let us consider that the contact with the rigid ground can occur at the corner A and at the corner B. The block is parametrized by the coordinates of the center of mass $[x, y]$ and the angle with respect to the ground θ , that is $q = [x, y, \theta]^T$. The unilateral constraints read as

$$\begin{cases} f_A(q) = y - \frac{1}{2} \cos \theta + \frac{1}{2} \sin \theta \geq 0, & \text{for the contact point A,} \\ f_B(q) = y - \frac{1}{2} \cos \theta - \frac{1}{2} \sin \theta \geq 0, & \text{for the contact point B.} \end{cases} \quad (9)$$

The equations of motion in the frictionless case are

$$\begin{cases} m\ddot{x} = 0, \\ m\ddot{y} = -mg + \lambda_A + \lambda_B, \\ I\ddot{\theta} = \lambda_A [\frac{1}{2} \sin \theta + \frac{1}{2} \cos \theta] + \lambda_B [\frac{1}{2} \sin \theta - \frac{1}{2} \cos \theta], \end{cases} \quad (10)$$

where m is the mass of the block and $I = \frac{m}{12}(l^2 + L^2)$ the inertia. Despite the fact that the Newton impact law might not be the most appropriate law for reproducing the rocking behavior of the block, we have chosen this example for the strong coupling between the contact points and the nonlinear constraints. Especially, the projection onto the constraints of one of the contact points can lead to a violation of the constraint for the other contact point if it has not been taken into account in a proper way.

2.2. Coulomb's friction

Let us consider now Coulomb's friction. In such a case when more complex contact laws are considered, the pure Lagrangian modeling of constraints is not sufficient. Indeed, the use of the Jacobian matrix of the constraints $G^T(t, q(t))$ in order to define the normal to the constraints is not necessarily convenient to introduce richer mechanical behaviors at the interface. Hence, we introduce for each contact α a local orthonormal frame at contact point C^α composed of a normal vector n^α and two tangent vectors t^α and s^α . In this frame, the local velocity at contact U^α and the reaction force λ^α are decomposed in its normal and tangent part as

$$\begin{aligned} U^\alpha &= U_N^\alpha n^\alpha + U_T^\alpha, & U_N^\alpha &\in \mathbb{R}, & U_T^\alpha &\in \mathbb{R}^2, \\ \lambda^\alpha &= \lambda_N^\alpha n^\alpha + \lambda_T^\alpha, & \lambda_N^\alpha &\in \mathbb{R}, & \lambda_T^\alpha &\in \mathbb{R}^2. \end{aligned} \quad (11)$$

Note that the operator $G(q)$ in (5) that links variables expressed in the local frame to generalized variables is not necessarily the gradient of some constraints.

Coulomb's friction is expressed in a disjunctive form as

$$\begin{cases} \text{if } U_T = 0 & \text{then } \lambda \in \mathbf{C} \\ \text{if } U_T \neq 0 & \text{then } \|\lambda_T\| = \mu|\lambda_N| \\ & \text{and there exists a scalar } a \geq 0 \text{ such that } \lambda_T = -aU_T \end{cases} \quad (12)$$

where $\mathbf{C} = \{\lambda, \|\lambda_T\| \leq \mu|\lambda_N|\}$ is the Coulomb friction cone. Let us introduce the modified velocity \hat{U} [13] defined by

$$\hat{U} = U + \mu \|U_T\| n. \quad (13)$$

With the Signorini condition at the velocity level, this notation provides us with a synthetic form of the Coulomb friction as

$$-\hat{U} \in N_C(\lambda), \quad (14)$$

where N_C is the normal cone to \mathbf{C} [45], or equivalently,

$$\mathbf{C}^* \ni \hat{U} \perp \lambda \in \mathbf{C}, \quad (15)$$

where $\mathbf{C}^* = \{v \in \mathbb{R}^n | r^T v \geq 0, \forall r \in \mathbf{C}\}$ is the dual cone of \mathbf{C} . For more details on this formulation and its theoretical interest, we refer to [5].

In this form, the numerical time integration of systems with Coulomb's friction is similar to case with only Signorini's condition written in terms of complementarity at the velocity level. The standard schemes and the new approaches developed in the sequel directly apply to the case with Coulomb's friction. To improve the readability, only the Signorini condition case will be detailed.

3. Time-integration methods for nonsmooth dynamics

Leaving aside the time-integration methods based on an accurate event detection procedure (event-tracking schemes or event-driven schemes [4, Chapter 8]), two main numerical schemes are available to date for integrating nonsmooth mechanical systems which are sound from the mathematical analysis point of view and which take advantage of a strong practical experience: the Moreau–Jean scheme and the Schatzman–Paoli scheme.

3.1. Moreau–Jean's scheme [35,26]

The Moreau–Jean scheme [35,26] is based on the Moreau sweeping process which enables to write the unilateral constraints at the velocity level including Newton's impact law,

$$\begin{cases} M(q(t))dv = F(t, q(t), v^+(t))dt + G(q(t))di, \\ \dot{q}(t) = v^+(t), \\ U(t) = G^T(q(t))v(t) \\ \text{if } g^\alpha(q(t)) \leq 0, \text{ then } 0 \leq U^{\alpha,+}(t) + eU^{\alpha,-}(t) \perp di \geq 0. \end{cases} \quad (16)$$

where dt is the Lebesgue measure, dv is a differential measure associated with v and di is an impulse reaction measure. When the evolution is smooth, the non-impulsive contact forces $\lambda(t)$ is considered as the density of di with respect to the Lebesgue measure, that is

$$\lambda(t) = \frac{di}{dt}(t). \quad (17)$$

The associated local reaction measure is defined by $dI = G(q)di$.

The numerical time integration of the measure differential inclusion (MDI) (16) is performed on an interval $(t_k, t_{k+1}]$ of length h as follows ($\theta \in [0, 1]$):

$$\begin{cases} M(q_{k+\theta})(v_{k+1} - v_k) - hF(t_{k+\theta}, q_{k+\theta}, v_{k+\theta}) = p_{k+1} = G(q_{k+1})P_{k+1}, & (18a) \\ q_{k+1} = q_k + hv_{k+\theta}, & (18b) \\ U_{k+1} = G^T(q_{k+1})v_{k+1} & (18c) \\ \text{if } \bar{g}_{k+1}^\alpha \leq 0 \text{ then } 0 \leq U_{k+1}^\alpha + eU_k^\alpha \perp P_{k+1}^\alpha \geq 0, \alpha \in \mathcal{I}, & (18d) \\ \text{otherwise } P_{k+1}^\alpha = 0. \end{cases}$$

where the following approximations are considered

$$\begin{aligned} v_{k+1} &\approx v^+(t_{k+1}); & U_{k+1} &\approx U^+(t_{k+1}); & p_{k+1} &\approx di(\{t_k, t_{k+1}\}); \\ P_{k+1} &\approx dI(\{t_k, t_{k+1}\}). \end{aligned} \quad (19)$$

The value \bar{g}_{k+1} is a prediction of the constraint that manages the activation at the velocity level. Several formulae for this forecast will be discussed in Section 4.4.

The numerical scheme which solves (16) enforces in discrete time the Newton impact law at each time step. On the contrary, the constraints in position $g(q(t)) \geq 0$ are not strictly satisfied. A violation of the constraints can occur at the activation of the contact and a drift of the constraints is generally observed if the constraints $g(q)$ is non linear.

3.2. Schatzman–Paoli's scheme [49,39,40]

The Schatzman–Paoli scheme [49,39,40] deals directly with the unilateral constraints $g(q(t)) \geq 0$ in discrete time and incorporates the Newton impact law such that the law is satisfied over two or

three time-steps. In this scheme, for $e = 0$, the position constraints is satisfied in discrete time but not the impact law.

For a non trivial mass matrix, in the multi-contact case and with a θ -method, the following scheme can be viewed as an extension of the original Schatzman–Paoli scheme

$$\begin{cases} M(q_{k+1})(q_{k+1} - 2q_k + q_{k-1}) - h^2 F(t_{k+\theta}, q_{k+\theta}, v_{k+\theta}) = p_{k+1}, & (20a) \\ v_{k+1} = \frac{q_{k+1} - q_{k-1}}{2h}, & (20b) \\ -p_{k+1} \in N_K\left(\frac{q_{k+1} + eq_{k-1}}{1+e}\right). & (20c) \end{cases}$$

For an admissible set defined by a finite set of unilateral constraints $K = \{q \in \mathbb{R}^n, y = g(q) \geq 0\}$,

the inclusion into the normal can be recast under some constraints qualification conditions as a nonlinear complementarity problem of the form

$$\begin{cases} g_{k+1} = g\left(\frac{q_{k+1} + eq_{k-1}}{1+e}\right), \\ p_{k+1} = G\left(\frac{q_{k+1} + eq_{k-1}}{1+e}\right)P_{k+1}, \\ 0 \leq g_{k+1} \perp P_{k+1} \geq 0. \end{cases} \quad (22)$$

The convergence of Schatzman–Paoli’s scheme is studied in [49,39,40,38] under various assumptions. When the impacts are perfectly inelastic ($e = 0$), we observe that the constraint $g(q_{k+1}) \geq 0$ is satisfied in discrete time.

3.3. Qualitative comparison of the schemes

For the sake of simplicity, let us consider a nonsmooth multi-body system subjected to simple linear constraints $q \geq 0$. Providing that M is symmetric positive definite in order to define an associated metric and using some basics in Convex Analysis [10], we can write:

$$\begin{aligned} M(x - y) - b &\in -\lambda N_K(x), \quad \lambda > 0, \\ &\Downarrow \\ x &= \operatorname{argmin}_{z \in K} \frac{1}{2}(z - y)^\top M(z - y) - (z - y)^\top b, \\ &\Downarrow \\ x &= \operatorname{prox}_M(K; y + M^{-1}b). \end{aligned} \quad (23)$$

Moreau–Jean’s time-stepping scheme can be written in terms of the proximal operator as

$$v_{k+1} + e v_k = \operatorname{prox}_{M(q_{k+1})}\left(T_{\mathbb{R}_+^n}(\tilde{q}_{k+1}); (1 + e)v_k + hM^{-1}(q_k + 1)F(t_{k+\theta}, q_{k+\theta}, v_{k+\theta})\right) \quad (24)$$

and Schatzman–Paoli’s scheme as

$$q_{k+1} + eq_{k-1} = \operatorname{prox}_{M(q_{k+1})}\left(\mathbb{R}_+^n; 2q_k - (1 - e)q_{k-1} + h^2 M^{-1}(q_k + 1)F(t_{k+\theta}, q_{k+\theta}, v_{k+\theta})\right). \quad (25)$$

From the qualitative point of view, the main difference between these two schemes is the mechanical nature of the projected variable. In the Moreau–Jean scheme, the variable which is projected is homogeneous to a velocity. One interesting remark is that the Newton impact law is respected for the discrete velocity in a very natural way by noting that

$$U_{k+1} = -eU_k \quad \text{if } P_{k+1} > 0. \quad (26)$$

This fact leads to a straightforward interpretation of the discrete multiplier as a mechanical impulse. However, the projection of the velocity onto the tangent cone of \mathbb{R}_+^n yields a slight violation of the constraints which occurs at the impact.

In the Schatzman–Paoli scheme, the generalized coordinates vector is directly projected onto the admissible set. The result is that there is no violation of the discrete constraints when $e = 0$. On the contrary, the discrete velocity does not satisfy the Newton impact law. Furthermore, the multiplier involved in the projection of the coordinates has no direct mechanical meaning. The Newton impact law is satisfied after several steps. On the other hand, on the simple linear oscillator example, the scheme does not generate artificial rebound in presence of flexibility.

4. A first solution: a direct projected scheme

In this section, we first propose a scheme which both satisfies in discrete time the position constraints and the velocity constraints, i.e., the impact law. This scheme is an adaption of the Moreau–Jean scheme based on the direct use of the Gear–Gupta–Leimkuhler (GGL) method [18]. Since this scheme will serve as the basis for an improved version in Section 5, we detail its local order of accuracy, its implementation, the choice of the activation rule and its main drawback: the chattering at contact.

4.1. General presentation of the direct projected scheme

Let us start by considering the following “augmented” system

$$\begin{cases} M(q(t))dv = F(t, q(t), v^+(t))dt + G(q(t))di, \\ \dot{q}(t) = v^+(t) + G(q(t))\mu(t), \\ U(t) = G^\top(q(t))v(t) \\ \text{if } g^z(q(t)) \leq 0, \text{ then } 0 \leq U^{z,+}(t) + eU^{z,-}(t) \perp di \geq 0, \\ 0 \leq g(q(t)) \perp \mu(t) \geq 0. \end{cases} \quad (27)$$

where $\mu(t)$ is a new multiplier which corresponds to the redundant constraints $g(q(t)) \geq 0$. Thanks to Moreau’s viability lemma[35], we expect that the multiplier is identically zero and that the solution of (27) is equivalent to the solution of (16). The proposed time-stepping scheme, called the *direct projected scheme* reads as

$$\begin{cases} M(q_{k+\theta})(v_{k+1} - v_k) - hF_{k+\theta} = G(q_{k+1})P_{k+1}, \\ q_{k+1} = q_k + hv_{k+\theta} + G(q_{k+1})\tau_{k+1}, \\ U_{k+1} = G^\top(q_{k+1})v_{k+1}, \\ g_{k+1} = g(q_{k+1}), \\ \text{if } g_{k+1}^z \leq 0, \text{ then } 0 \leq U_{k+1}^z + eU_k^z \perp P_{k+1}^z \geq 0. \\ 0 \leq g_{k+1} \perp \tau_{k+1} \geq 0. \end{cases} \quad (28)$$

The discrete multiplier

$$\tau_{k+1} \approx \int_{t_k}^{t_{k+1}} \mu(t) dt \quad (29)$$

ensures the constraints at the position level in discrete time $g_{k+1} \geq 0$.

4.2. Empirical convergence and order analysis

The global order of the scheme is shown on the two very simple systems described in Examples 1 and 2. For the sake of simplicity we choose for the prediction of the constraints the fully explicit forecast: $\bar{g}_{k+1} = g_k$. Other choices will be discussed in Section 4.4. Fig. 2 shows the global order of convergence of the direct projected scheme follows the order of the Moreau–Jean scheme and the Paoli–Schatzman scheme. We can notice that the projection does not improve the global quality of the solution. Let us now study the local order of accuracy of the scheme and let us start with the discrete multiplier τ . On Fig. 3, it is shown that the discrete

multiplier τ_{k+1} is of order $\mathcal{O}(h)$. This result is proven in Proposition 1 under the following assumptions:

Assumption 1 (Existence and uniqueness). A unique global solution over $[0, T]$ for augmented Moreau's sweeping process (27) is assumed such that $q(\cdot)$ is absolutely continuous and admits a right velocity $v^+(\cdot)$ at every instant t of $[0, T]$ and such that the function $v^+ \in LBV([0, T], \mathbb{R}^n)$.

Assumption 2 (Smoothness of data). The following smoothness on the data will be assumed: (a) the inertia operator $M(q)$ is assumed to be of class C^0 and definite positive, (b) the force mapping $F(t, q, v)$ is assumed to be of class C^0 , (c) the constraint functions $g(q)$ are assumed to be of class C^1 and (d) the Jacobian matrix $G^T(q) = \nabla_q^T g(q)$ is assumed to have full-row rank.

Proposition 1. Under Assumptions 1 and 2, the multiplier τ_{k+1} is of order h that is

$$\tau_{k+1} = \mathcal{O}(h). \tag{30}$$

Proof. Let us consider the first order Taylor expansion of the constraints, $g(q)$ at q_k

$$\begin{aligned} g_{k+1} &= g(q_{k+1}) = g(q_k) + \nabla_q^T g(q_k)(q_{k+1} - q_k) + \mathcal{O}(\|q_{k+1} - q_k\|^2) \\ &= g(q_k) + G^T(q_k)[h v_{k+\theta} + G(q_{k+1})\tau_{k+1}] + \mathcal{O}(\|q_{k+1} - q_k\|^2) \\ &= g(q_k) + hG^T(q_k)v_{k+\theta} + G^T(q_k)G(q_{k+1})\tau_{k+1} + \mathcal{O}(\|q_{k+1} - q_k\|^2). \end{aligned} \tag{31}$$

Let us denote the index sets of active constraints by $\beta = \{i | \tau_{k+1}^i > 0\}$. Since $g_{k+1}^\beta = 0$ and G has full row rank, the solution of the LCP can be written as

$$\tau_{k+1}^\beta = -[G^T(q_k)G(q_{k+1})]_{\beta\beta}^{-1} [g^\beta(q_k) + hG_{\beta\bullet}^T(q_k)v_{k+\theta} + \mathcal{O}(\|q_{k+1} - q_k\|^2)]. \tag{32}$$

Since $g_{k+1}^\beta = 0$, we also obtain

$$\begin{aligned} g^\beta(q_k) &= -\nabla_q^T g(q_k)(q_{k+1} - q_k) + \mathcal{O}(\|q_{k+1} - q_k\|^2) \\ &= \mathcal{O}(\|q_{k+1} - q_k\|). \end{aligned} \tag{33}$$

From (32) and (33), we get the following estimate

$$\tau_{k+1}^\beta = -[G^T(q_k)G(q_{k+1})]_{\beta\beta}^{-1} [hG_{\beta\bullet}^T(q_k)v_{k+\theta} + \mathcal{O}(\|q_{k+1} - q_k\|)] \tag{34}$$

and more generally, since $\tau_{k+1}^i = 0$ for $i \notin \beta$, we get

$$\tau_{k+1} = \mathcal{O}(\|q_{k+1} - q_k\|) + \mathcal{O}(h). \tag{35}$$

since $v_{k+\theta}$ is assumed to be bounded. Inserting this estimate in

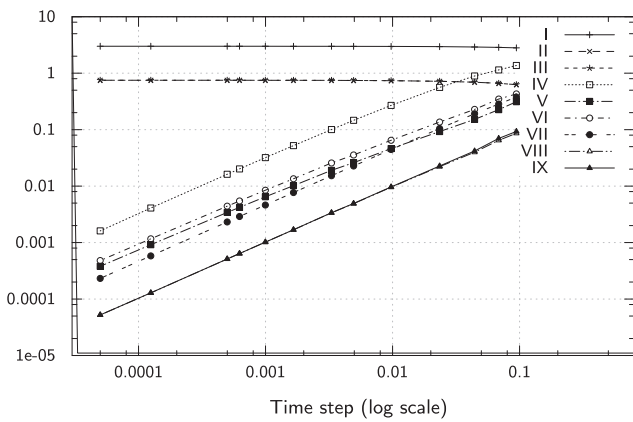
$$q_{k+1} - q_k = h v_{k+\theta} + G(q_{k+1})\tau_{k+1}, \tag{36}$$

we get that

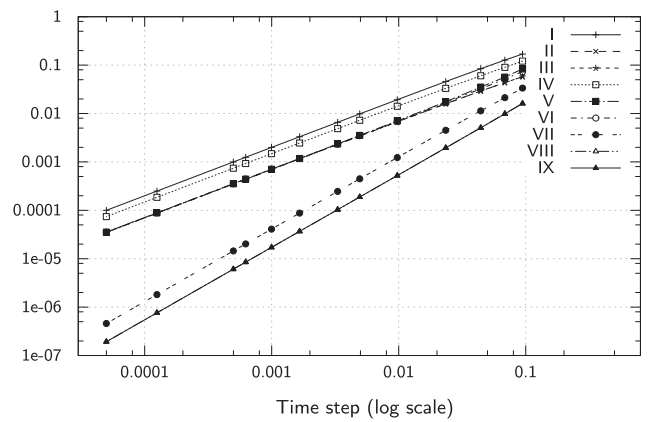
$$\mathcal{O}(\|q_{k+1} - q_k\|) = \mathcal{O}(h) \tag{37}$$

and we conclude that $\tau_{k+1} = \mathcal{O}(h)$. \square

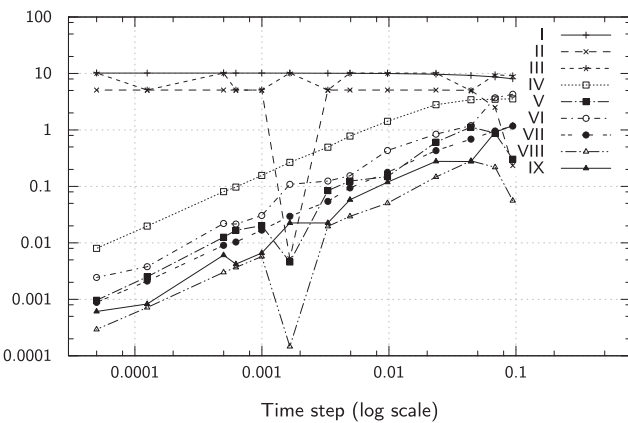
The following result is a straightforward extension of the Proposition 1 in [3].



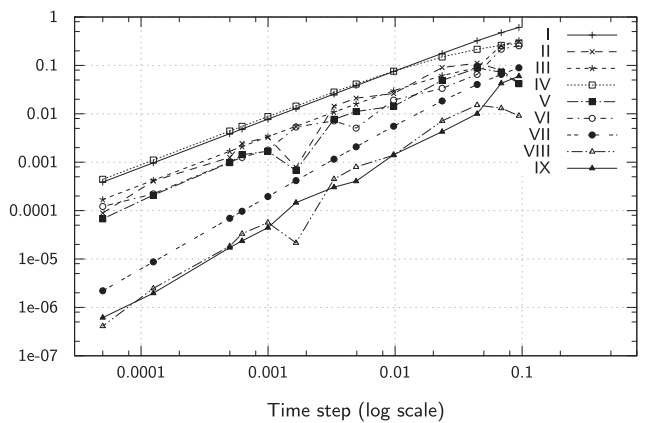
(a) The bouncing ball (Example 1). Velocity error



(b) The bouncing ball (Example 1). Coordinate error

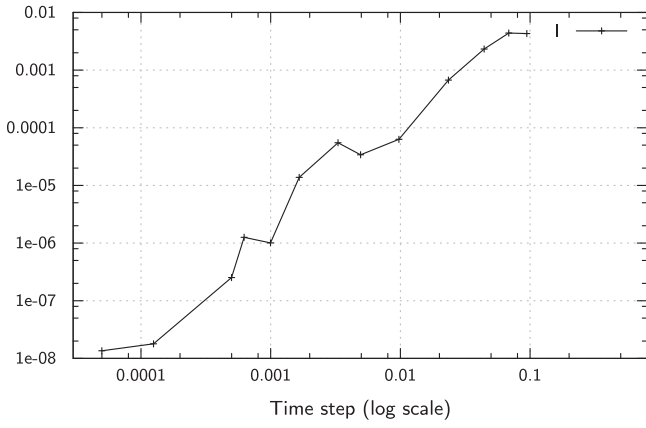


(c) The linear oscillator (Example 2). Velocity error

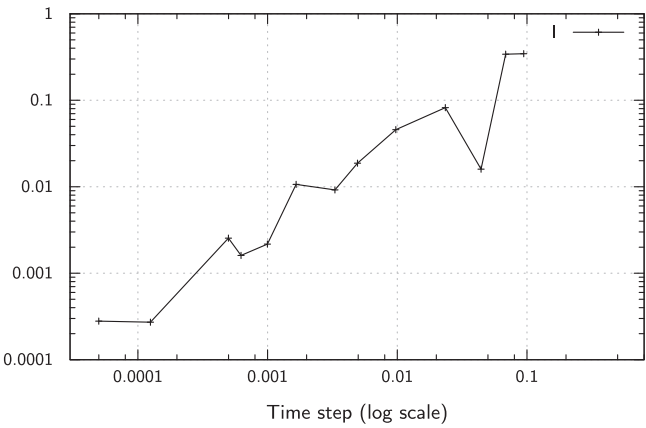


(d) The linear oscillator (Example 2). Coordinate error

Fig. 2. Empirical order of convergence of time-stepping schemes. Paoli–Schatzman scheme: (I) uniform norm, (IV) l_1 norm, (VII) l_2 norm. Moreau–Jean's scheme: (II) uniform norm, (V) l_1 norm, (VIII) l_2 norm. Direct projected scheme (28). (III) uniform norm, (VII) l_1 norm, (IX) l_2 norm.



(a) The bouncing ball (Example 1). $\max_k(\|\tau_k\|)$



(b) The linear oscillator (Example 2). $\max_k(\|\tau_k\|)$

Fig. 3. (l) Magnitude of the multiplier τ_{k+1} with respect to the time step size for the direct projected scheme (28).

Proposition 2. Under Assumptions 1 and 2, the local order of consistency of the Moreau–Jean time-stepping scheme with projection for the generalized coordinates is $e_q = \mathcal{O}(h)$ and at least for the velocities $e_v = \mathcal{O}(1)$.

Proof. The estimate e_v on the velocity is trivial if we recall that $M_{k+\theta}^{-1}(F_{k+\theta} + p_{k+1})$ is bounded on $[t_k, t_{k+1}]$. The BV function $v(\cdot)$ is also bounded on $[t_k, t_{k+1}]$ then we have that e_v is also bounded. Therefore, we obtain $e_v = \mathcal{O}(1)$. Using Lemma 1 in [3] for $v^+ \in BV(I, \mathbb{R}^n)$, we get

$$\left\| \int_{t_k}^{t_{k+1}} v(s) ds - h(\theta v^+(t_{k+1}) + (1-\theta)v^+(t_k)) \right\| \leq C(\theta)h \text{var}(v^+, I), \quad (38)$$

with $C(\theta) = \theta$ if $\theta \geq 1/2$ and $C(\theta) = 1 - \theta$ otherwise. Since $v_k = v^+(t_k)$ and $v_{k+1} = v(t_{k+1}) + \mathcal{O}(1)$, we obtain for (38)

$$\left\| \int_{t_k}^{t_{k+1}} v(s) ds - h(\theta v_{k+1} + (1-\theta)v_k) - \theta \mathcal{O}(h) \right\| = \|e_q + G(q_{k+\theta})\tau_{k+1} - \theta \mathcal{O}(h)\| \leq C(\theta)h \text{var}(v^+, I). \quad (39)$$

Using the result of Proposition 1, $\tau_{k+1} = \mathcal{O}(h)$, we get

$$\|e_q + \mathcal{O}(h)\| \leq C(\theta)h \text{var}(v^+, I), \quad (40)$$

which completes the proof. \square

4.3. Implementation

In this section, several possible implementations and variants of the direct projected scheme (28) are detailed. Let first us discuss the strict implementation of (28). The nonlinear residual function is defined as

$$\mathcal{R}(v, q) = \begin{bmatrix} M(\theta q + (1-\theta)q_k)(v - v_k) \\ -hF(t_{k+\theta}, \theta q + (1-\theta)q_k, \theta v + (1-\theta)v_k) - G(q)P_{k+1} \\ q - q_k - h(\theta v + (1-\theta)v_k) - G(q)\tau_{k+1} \end{bmatrix}. \quad (41)$$

For given values of P_{k+1} and τ_{k+1} , the unknowns v_{k+1} and q_{k+1} which solve the first two lines of (28) satisfy $\mathcal{R}(v_{k+1}, q_{k+1}) = 0$. This set of nonlinear equations can be solved by standard solvers [37]. For Newton's method, the solution is sought as a limit of the sequence $\{v^n, q^n\}_{n \in \mathbb{N}}$ such that

$$\begin{cases} v^0 = v_k, & q^0 = q_k, \\ \mathcal{R}_L(v^{n+1}, q^{n+1}) \triangleq \mathcal{R}(v^n, q^n) + \nabla_v \mathcal{R}(v^n, q^n)(v^{n+1} - v^n) \\ \quad + \nabla_q \mathcal{R}(v^n, q^n)(q^{n+1} - q^n) = 0. \end{cases} \quad (42)$$

In order to be self-contained but without enter into deepest details, we will describe a semi-Newton procedure in which the inertia matrix and the Jacobian of the constraints are only updated in a fixed point way and then evaluated at (v^n, q^n) . It amounts to neglecting the Jacobian of M and G in the Newton loop. We solve

$$\mathcal{R}(v^n, q^n) + \begin{bmatrix} M(q_\theta^n) - h\theta \nabla_v F(t_{k+\theta}, q_\theta^n, v_\theta^n) \\ -h\theta I_{n \times n} \end{bmatrix} (v^{n+1} - v^n) + \begin{bmatrix} -h\theta \nabla_q F(t_{k+\theta}, q_\theta^n, v_\theta^n) \\ I_{n \times n} \end{bmatrix} (q^{n+1} - q^n) = 0. \quad (43)$$

where q_θ^n (resp. v_θ^n) denotes $\theta q^n + (1-\theta)q_k$ (resp. $\theta v^n + (1-\theta)v_k$) and $M^n = M(q_\theta^n)$. Let us denote the values of P_{k+1} and τ_{k+1} at the Newton iteration n by P^{n+1} and τ^{n+1} . After simple algebraic manipulations, we obtain

$$\begin{cases} [M^n + h\theta C^n](v^{n+1} - v^n) = -h\theta K^n(q^{n+1} - q^n) - M(q_\theta^n)(v^n - v_k) \\ \quad + hF(t_{k+\theta}, q_\theta^n, v_\theta^n) + G(q^n)P^{n+1}, \\ q^{n+1} = q_k + h v_\theta^{n+1} + G(q^n)\tau^{n+1}, \end{cases} \quad (44)$$

where $C^n = -\nabla_v F(t_{k+\theta}, q_\theta^n, v_\theta^n)$ denotes the tangent damping matrix and $K^n = -\nabla_q F(t_{k+\theta}, q_\theta^n, v_\theta^n)$ the tangent stiffness matrix. A substitution in (44) of the second equation into the first one yields

$$\begin{cases} [M^n + h\theta C^n + h^2 \theta^2 K^n](v^{n+1} - v^n) = \\ \quad -M(q_\theta^n)(v^n - v_k) + hF(t_{k+\theta}, q_\theta^n, v_\theta^n) + h\theta K^n(q_k - q^n + h(1-\theta)v_k) \\ \quad + h\theta K^n G(q^n)\tau^{n+1} + G(q^n)P^{n+1}, \\ q^{n+1} = q_k + h v_\theta^{n+1} + G(q^n)\tau^{n+1}. \end{cases} \quad (45)$$

In condensed matrix notation we obtain

$$\begin{bmatrix} \hat{M} & 0 \\ h & I \end{bmatrix} \begin{bmatrix} v^{n+1} - v^n \\ q^{n+1} - q^n \end{bmatrix} = \begin{bmatrix} f \\ -h v^n \end{bmatrix} + \begin{bmatrix} G(q^n) & h\theta K^n G(q^n) \\ 0 & G(q^n) \end{bmatrix} \begin{bmatrix} P^{n+1} \\ \tau^{n+1} \end{bmatrix}, \quad (46)$$

with the iteration matrix \hat{M} defined by

$$\hat{M} = [M^n + h\theta C^n + h^2 \theta^2 K^n] \quad (47)$$

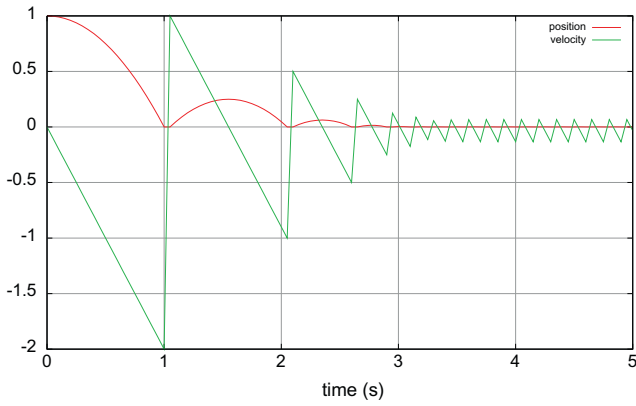
and

$$f = -M^n(v^n - v_k) + hF(t_{k+\theta}, q_\theta^n, v_\theta^n) + h\theta K^n(q_k - q^n + h(1-\theta)v_k). \quad (48)$$

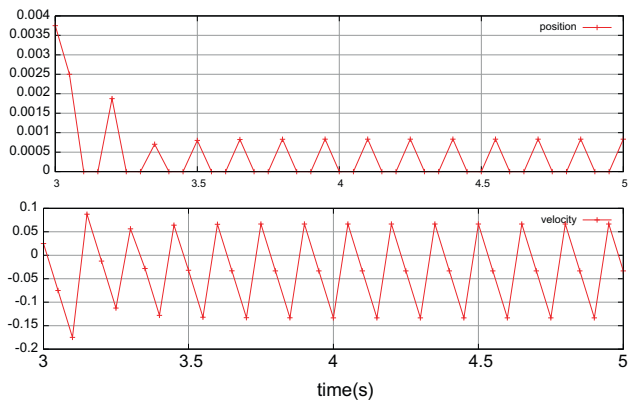
The nonlinear constraints $g(q_{k+1}) \geq 0$ are also linearized by considering the following nonlinear residual function

$$\mathcal{R}_g(y, q) = y - g(q) \quad (49)$$

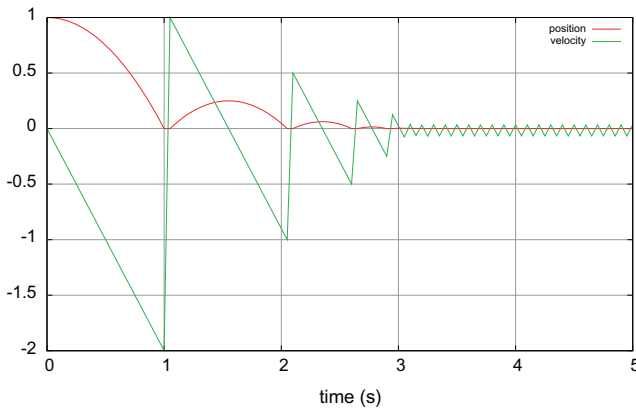
and its first order expansion,



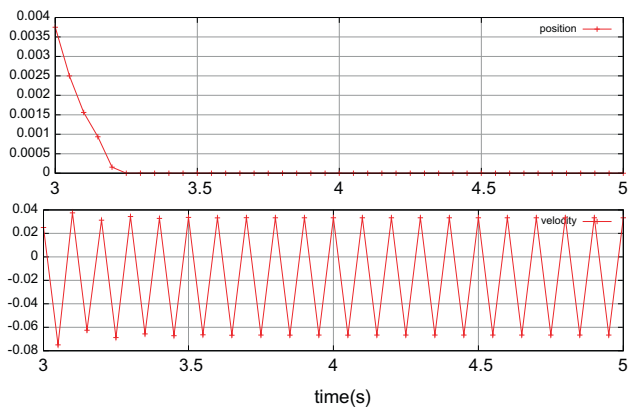
(a) Explicit position forecast (61) with $\gamma = 0$



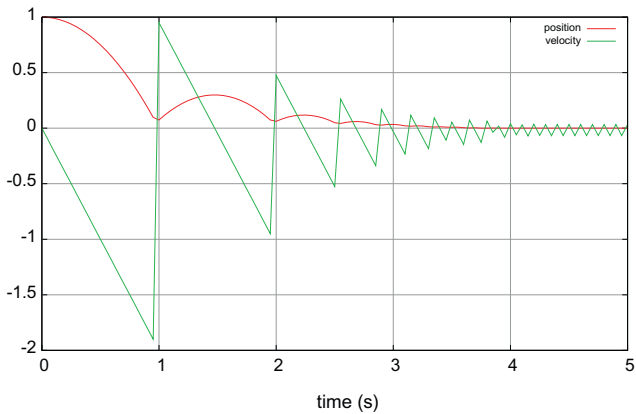
(b) Zoom on $t \in [3, 5]$ for $\gamma = 0$



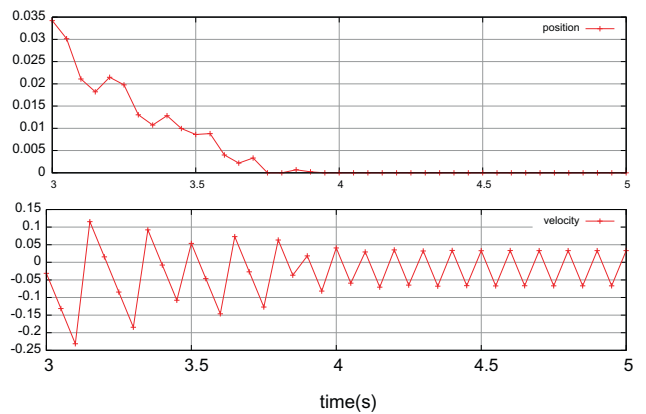
(c) Explicit position forecast (61) with $\gamma = 1$



(d) Zoom on $t \in [3, 5]$ for $\gamma = 1$



(e) Explicit position forecast (61) with $\gamma = 2$



(f) Zoom on $t \in [3, 5]$ for $\gamma = 2$

Fig. 4. The chattering behavior for the bouncing ball (Example 1) with the explicit position forecast (61). Position and velocity vs. time for $h = 5 \times 10^{-2}$.

$$\mathcal{R}_{g,L}(y^{n+1}, q^{n+1}) \triangleq y^n - g(q^n) - G^\top(q^n)(q^{n+1} - q^n) + y^{n+1} - y^n. \quad (50)$$

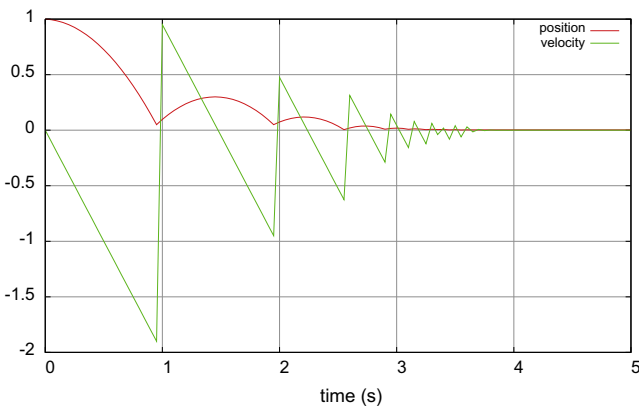
By denoting $y^{n+1} = g^{n+1}$, we get the following system of linearized constraints

$$g^{n+1} = g(q^n) + G^\top(q^n)(q^{n+1} - q^n) \geq 0. \quad (51)$$

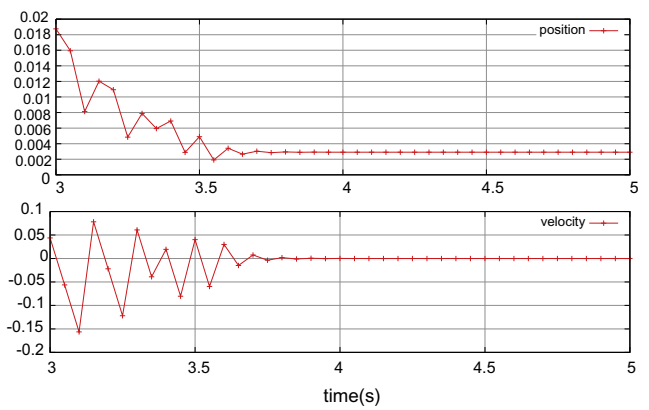
Let us note the set of active constraints in velocity by $\mathcal{I}_v = \{\alpha | \bar{g}_{k+1}^\alpha \leq 0\}$. The unknown local velocity vector at step n for this set of constraints is shortly denoted as written as $U^{n+1} = [U^{\top, n+1, \alpha}, \alpha \in \mathcal{I}_v]^\top$. The following Mixed Linear Complementarity Problem (MLCP) must be solved at each Newton's loop

$$\begin{bmatrix} \hat{M} & 0 & 0 & 0 \\ h & I & 0 & 0 \\ -G^\top(q^n) & 0 & I & 0 \\ 0 & -G^\top(q^n) & 0 & I \end{bmatrix} \begin{bmatrix} v^{n+1} - v^n \\ q^{n+1} - q^n \\ U^{n+1} - U^n \\ g^{n+1} \end{bmatrix} = \begin{bmatrix} f \\ -h v^n \\ 0 \\ g(q^n) \end{bmatrix} + \begin{bmatrix} G(q^n) & h\theta K^n G(q^n) \\ 0 & G(q^n) \\ 0 & 0 \\ 0 & 0 \end{bmatrix} \begin{bmatrix} P^{n+1} \\ \tau^{n+1} \end{bmatrix}, \quad (52)$$

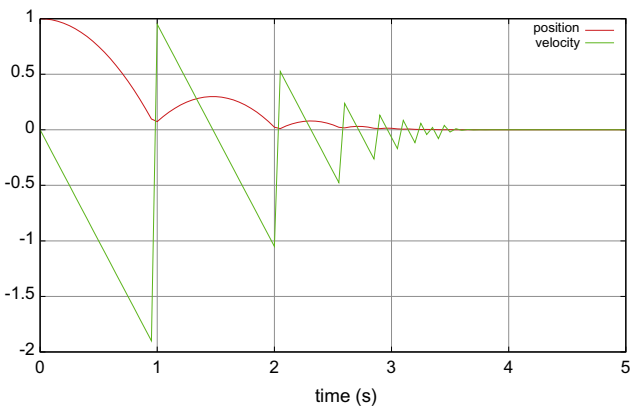
$$0 \leq U^{n+1} \perp P^{n+1} \geq 0, \quad 0 \leq g^{n+1} \perp \tau^{n+1} \geq 0.$$



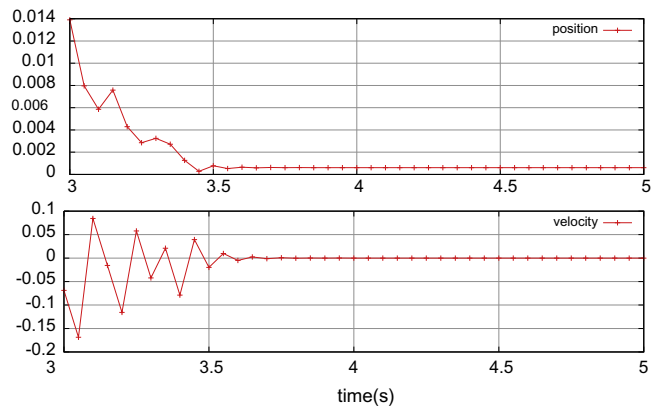
(a) Free position forecast (62) with $\theta = 1$



(b) Zoom on $t \in [3, 5]$ with $\theta = 1$



(c) Free position forecast (62) with $\theta = 1/2$



(d) Zoom on $t \in [3, 5]$ with $\theta = 1/2$

Fig. 5. Chattering-free behavior for the bouncing ball (Example 1) with the free position forecast (62). Position and velocity vs. time for $h = 5 \times 10^{-2}$.

for v^{n+1} , U^{n+1} , P^{n+1} , g^{n+1} , τ^{n+1} . Since the first matrix in (52) is lower block triangular and invertible if \widehat{M} is invertible, we can build a condensed Linear Complementarity Problem (LCP) as follows

$$\begin{cases} \begin{bmatrix} U^{n+1} \\ g^{n+1} \end{bmatrix} = W \begin{bmatrix} P^{n+1} \\ \tau^{n+1} \end{bmatrix} + a, \\ 0 \leq U^{n+1} \perp P^{n+1} \geq 0, \\ 0 \leq g^{n+1} \perp \tau^{n+1} \geq 0, \end{cases} \quad (53)$$

with

$$W = \begin{bmatrix} G^T(q^n) \widehat{M}^{-1} G(q^n) & h^2 \theta^2 G^T(q^n) \widehat{M}^{-1} K^n \\ h \theta G^T(q^n) \widehat{M}^{-1} G(q^n) & G^T(q^n) G(q^n) + h^2 \theta^2 G^T(q^n) \widehat{M}^{-1} K^n \end{bmatrix} \quad (54)$$

and

$$a = \begin{bmatrix} U^n + G^T(q^n) \widehat{M}^{-1} f \\ g(q^n) + G^T(q^n) [q_k - q^n + h \theta (v^n + \widehat{M}^{-1} f)] \end{bmatrix}. \quad (55)$$

4.3.1. A decoupled implementation

In this section, we propose a simplified implementation of the method by updating higher order terms in h in the Newton iterations in a fixed point way. Let us consider the following modified version of (45):

$$\begin{cases} [M(q_\theta^n) + h \theta C^n + h^2 \theta^2 K^n] (v^{n+1} - v^n) = \\ -M(q_\theta^n) (v^n - v_k) + h F(t_{k+\theta}, q_\theta^n, v_\theta^n) \\ + h \theta K^n (q_k - q^n + h(1 - \theta) v_k) + h \theta K^n G(q^n) \tau^n + G(q^n) P^{n+1} \\ q^{n+1} = q_k + h v_\theta^{n+1} + G(q^n) \tau^{n+1}. \end{cases} \quad (56a) \quad (56b)$$

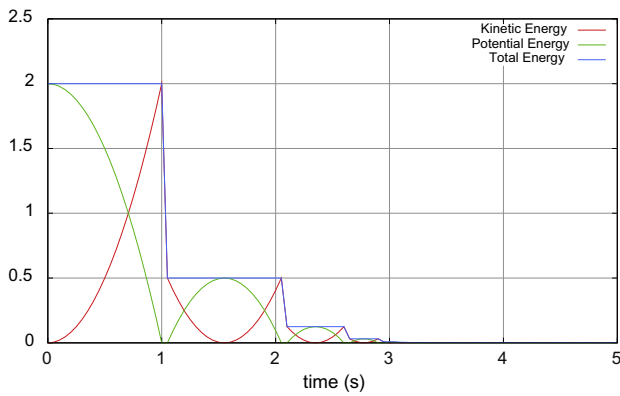
Note that the value of τ_{k+1} in the right hand side of the equation is taken at step n that is τ^n . Doing that way, the following LCP can be first solved

$$\begin{cases} U^{n+1} = [G^T(q^n) \widehat{M}^{-1} G(q^n)] P^{n+1} \\ + [U^n + G^T(q^n) \widehat{M}^{-1} b + h \theta G^T(q^n) K^n G(q^n) \tau^n], \\ 0 \leq U^{n+1} \perp P^{n+1} \geq 0. \end{cases} \quad (57)$$

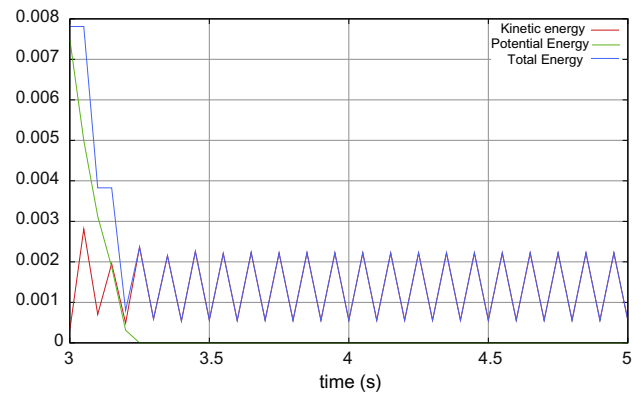
Knowing the value P^{n+1} , hence the value of v^{n+1} given by (56a), a second LCP is solved as follows

$$\begin{cases} q^{n+1} = [G^T(q^n) G(q^n)] \tau^{n+1} + h v_\theta^{n+1}, \\ 0 \leq q^{n+1} \perp \tau^{n+1} \geq 0. \end{cases} \quad (58)$$

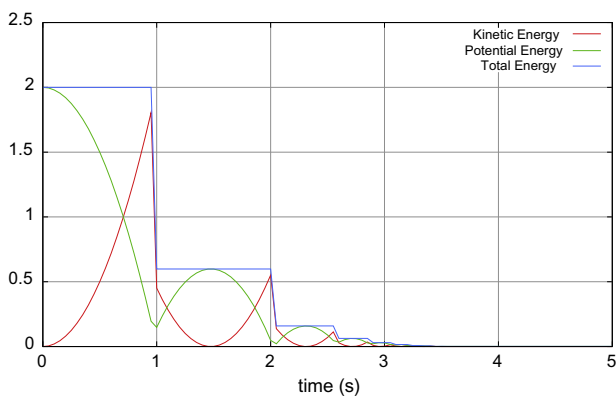
The main interest of this decoupled implementation lies in the formulation of two smaller LCPs (57) and (58) rather than the larger one (53). Furthermore, the matrix involved in the first LCP at the velocity level (57) is identical to the LCP matrix that is used in the standard Moreau–Jean scheme. This decoupled implementation needs only two slight modifications of the standard Moreau–Jean scheme adding a new term in the right hand side of (56a) and



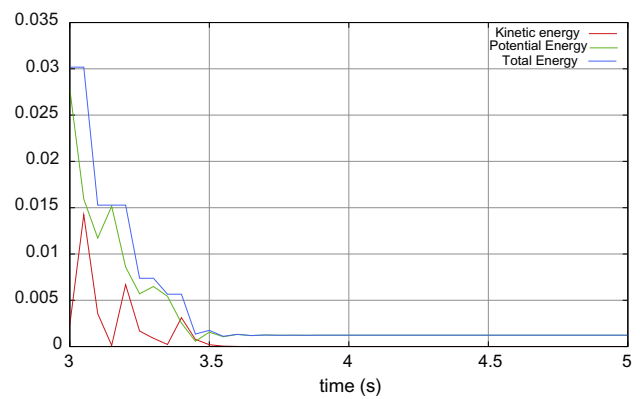
(a) Energy diagram with $\theta = 1/2$. $\gamma = 1$



(b) Zoom on $t \in [3, 5]$ Energy diagram with $\theta = 1/2$. $\gamma = 1$

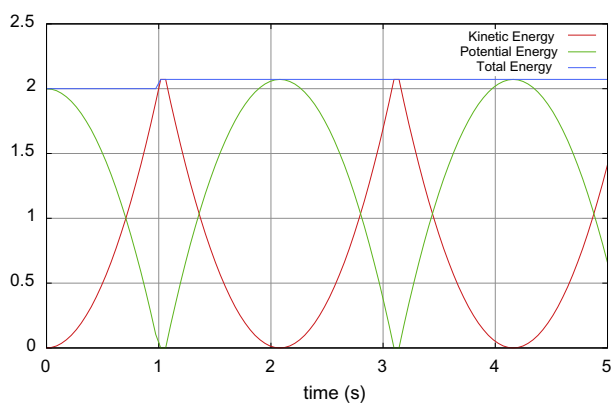


(c) Energy diagram with $\theta = 1/2$. Free position forecast (62).

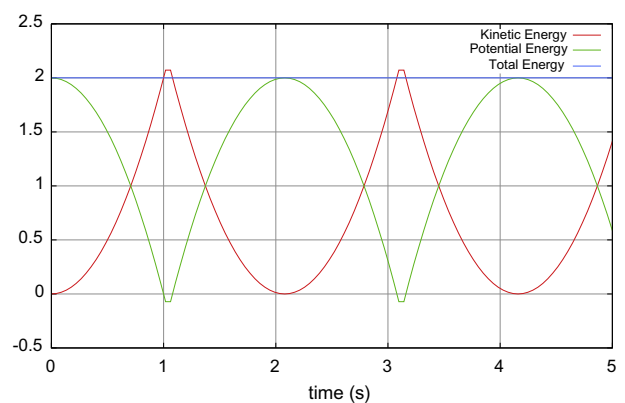


(d) Zoom on $t \in [3, 5]$ Energy diagram with $\theta = 1/2$. Free position forecast (62).

Fig. 6. Energy for the bouncing ball (Example 1). $h = 5 \times 10^{-2}$.



(a) Energy diagram $\theta = 1/2$ with projection



(b) Energy diagram $\theta = 1/2$ without projection

Fig. 7. Energy in the elastic case ($e = 1$) for the bouncing ball (Example 1). $h = 5 \times 10^{-2}$.

performing the decoupled projection by solving the LCP (58). The algorithm is detailed in Algorithm 1.

Remark 3. It can also be interesting to consider the following rule for the correction of the position

$$\dot{q}(t) = v^+(t) + N(q(t))G(q(t))\mu(t), \quad (59)$$

where $N(q) \in \mathbb{R}^{n \times n}$ is a positive definite matrix. It amounts to choosing a special metric or the projection onto the constraints. Since the projection of the velocity is based on the kinetic metric, it may be convenient to select the same kind of projection for the position. Applying the proposed discretization and the decoupled implementation, the following LCP equivalent to (58) is obtained

$$\begin{cases} q^{n+1} = [G^T(q^n)N(q^n)G(q^n)]\tau^{n+1} + hv_\theta^{n+1}, \\ 0 \leq q^{n+1} \perp \tau^{n+1} \geq 0. \end{cases} \quad (60)$$

Choosing the $N(q^n) = \widehat{M}^{-1}$ allows one to form the same matrix for the first LCP in velocity and the second one in position.

In the numerical practise the decoupled implementation performs very efficiently. This is mainly due to the fact that the neglected coupling terms are of order h^2 and hence have a weak influence in the behavior of the scheme. Therefore, the decoupling strategy does only slightly change the average number of Newton's iterations and fixed point iterations (see Table 3 for an example).

4.3.2. Convergence criteria

The convergence of the scheme with the coupled or decoupled implementation is ensured by checking against the prescribed tolerance the norm of the residual term (41) $\mathcal{R}(v^{n+1}, q^{n+1})$ and the residual term (49) $\mathcal{R}_g(g^{n+1}, q^{n+1})$. Furthermore, we check that the complementarity conditions are satisfied inside the LCP solver.

Algorithm 1. Direct Projected Algorithm for one time-step (decoupled implementation).

Require: h time-step, $I = [t_k, t_{k+1}]$, $tol \in \mathbb{R}$ a user tolerance

Require: q_k, v_k initial values of the step.

Ensure: $q_{k+1}, v_{k+1}, P_{k+1}, \tau_{k+1}$

// update the index Set

$\mathcal{I}_v \leftarrow \{\alpha | \bar{g}_{k+1}^\alpha \leq 0\}$ with one the rule Eq. (61) or (62).

$v^n \leftarrow v_k; q^n \leftarrow q_k; P^n \leftarrow 0; \tau^n \leftarrow 0$

// Start Newton's loop

while $\mathcal{R}(v^{n+1}, q^{n+1}) > tol$ **or** $\mathcal{R}_g(g^{n+1}, q^{n+1}) > tol$

// Solve the first LCP (Eq. (57)) for U^{n+1} and P^{n+1} .

$$\begin{cases} U^{n+1} = [G^T(q^n)\widehat{M}^{-1}G(q^n)]P^{n+1} \\ + [U^n + G^T(q^n)\widehat{M}^{-1}b + h\theta G^T(q^n)K^nG(q^n)\tau^n] \\ 0 \leq U^{n+1} \perp P^{n+1} \geq 0 \end{cases}$$

// Update the velocity v^{n+1} (Eq. (56a))

$$\begin{aligned} & [M(q_\theta^n) + h\theta C^n + h^2\theta^2 K^n](v^{n+1} - v^n) \\ & = -M(q_\theta^n)(v^n - v_k) + hF(t_{k+\theta}, q_\theta^n, v_\theta^n) + h\theta K^n(q_k - q^n + h(1 \\ & - \theta)v_k) + h\theta K^n G(q^n)\tau^n + G(q^n)P^{n+1} \end{aligned}$$

// Solve the second LCP (Eq. (58)) for q^{n+1} and τ^{n+1} .

$$\begin{cases} q^{n+1} = [G^T(q^n)G(q^n)]\tau^{n+1} + hv_\theta^{n+1} \\ 0 \leq q^{n+1} \perp \tau^{n+1} \geq 0 \end{cases}$$

$n \leftarrow n + 1$

end while

$v_{k+1} \leftarrow v^n, P_{k+1} \leftarrow P^n$

$q_{k+1} \leftarrow q^n, \tau_{k+1} \leftarrow \tau^n$

4.4. How to choose a good prediction scheme for the activation of constraints?

In this section, we discuss the prediction of the constraints, i.e., the computation of the value of \bar{g}_{k+1} . The choice of the forecast \bar{g}_{k+1} will be discussed in details as it plays a leading part in the global behavior of the scheme. The following implementation will be discussed:

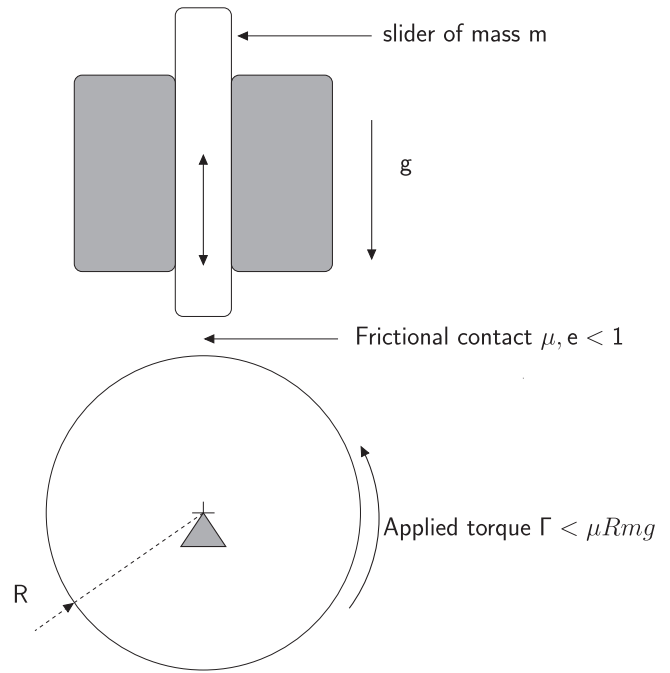


Fig. 8. A slider and roller example.

- The fully *explicit forecast* consists in evaluating the constraints with the values of the previous time-step,

$$\bar{g}_{k+1} = g_k + \gamma h U_k, \quad (61)$$

where γ is usually chosen in $[0, 2]$. The main interest of this method lies in its simplicity. For $\gamma = 0$, the constraints on velocity are activated when the constraints in position are violated. Without projection, this rule is very robust, but may yield negative violations of order $\mathcal{O}(h)$. For $\gamma > 0$, this scheme uses an extrapolation of the trajectory to guess if a constraint will be violated within the time-step. Let us recall that if the trajectory is absolutely continuous, the velocity is not. Therefore, the extrapolation can not be better than $\mathcal{O}(h)$. One of the interest of this approach is an activation of the constraints can be set before the violation of the constraints. Unfortunately, as the constraints are treated at the velocity level, a reaction force can be imposed even if $g_{k+1} > 0$. The only thing that can be said is that $g_{k+1} = \mathcal{O}(h)$.

- The *free-position forecast* is based on the evaluation of the position without any reaction forces due to unilateral constraints, that is

$$\bar{g}_{k+1} = g_k + h(\theta U_{\text{free}} + (1 - \theta)U_k), \quad (62)$$

where U_{free} is the relative free velocity at contact and the parameter θ is chosen such that $\theta \in (0, 1]$.

Remark 4. The question of a *semi-implicit forecast* based on the update of the position inside the Newton loop without the projection onto the constraints, i.e.

$$g_{k+1} = g(q_k + hv_{k+\theta}^z) \quad (63)$$

or a fully *implicit forecast* based on the implicit evaluation of the position without the projection onto the constraints, that is

$$g_{k+1} = g(q_k + hv_{k+\theta}) \quad (64)$$

is a difficult question. Since the activation of the constraints will modify the velocity at the end of the step, the previous choices in (63) and (64) are most of time inconsistent and yields the cycling

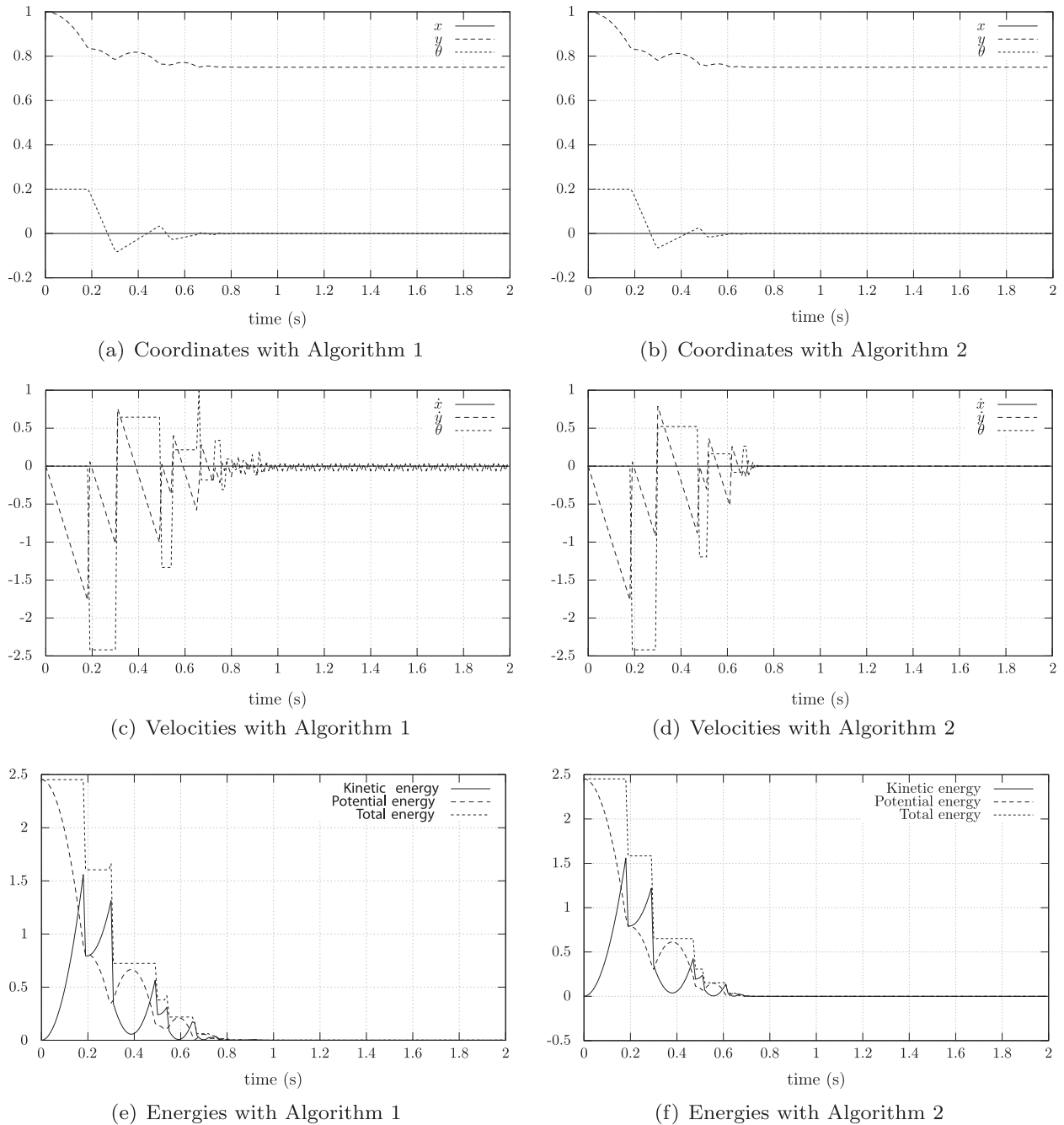


Fig. 9. The rocking block (Example 3). Comparison of the direct projection scheme (Algorithm 1) and the combined activation/projection approach (Algorithm 2).

in the activation of constraints without any convergence. However, we will see in Section 5 how such a similar idea can be used without cycling by augmenting in a unique way the set of active constraints.

4.5. Artificial oscillations, chattering and energy balance

Let us study the behavior of the projected scheme (28) together with the explicit forecast (61) on the bouncing ball Example 1. In Fig. 4, a cycling behavior is observed after the finite accumulation when the ball would come to rest on the ground. This behavior was already observed in [54]. One of the explanation is that the energy brought to the system by the projection exactly compensates the energy dissipated during the impact. One of the consequences of this cycle is that the contact is never stabilized and the reaction

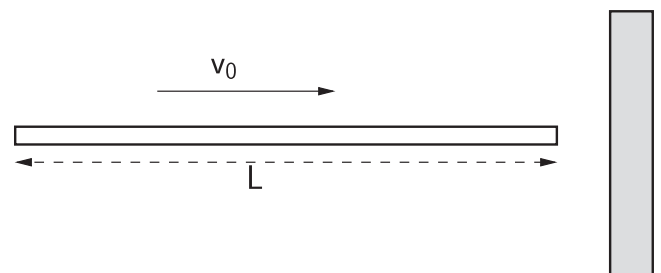


Fig. 10. The elastic impacting bar problem.

forces does not converge towards the constant value which counteracts the weight of the ball.

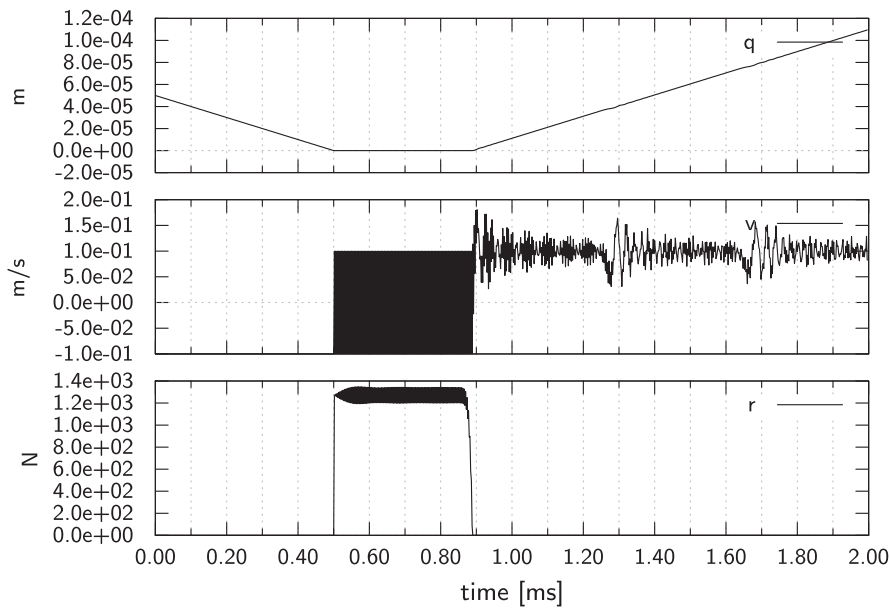


Fig. 11. Trapezoidal rule with a position-based constraints. Position q , velocity v and reaction force r at the contact point. $h = 2 \times 10^{-06}$ s. Number of elements $N = 1000$.

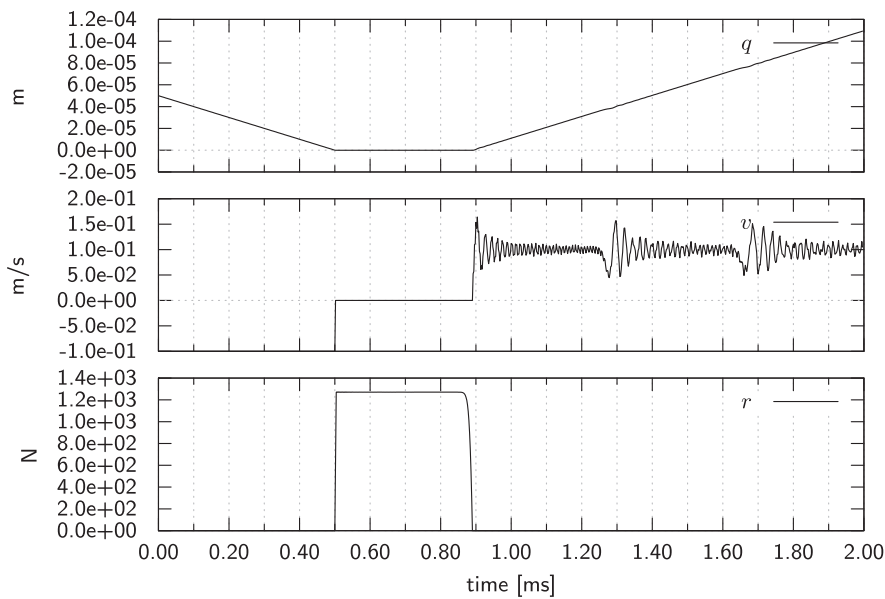


Fig. 12. Moreau-Jean scheme. Position q , velocity v and reaction force r at the contact point. $\theta = 1/2$, $h = 5 \times 10^{-05}$ s. Number of elements $N = 1000$.

Note that the chattering is observed in Fig. 4 whatever the choice of the prediction parameter γ in (61). However, we note in Fig. 5 that the chattering is not observed with the free position forecast (62). Indeed, when this latter forecast rule is used on the bouncing ball example, the constraint is never violated, i.e. $g_{k+1} > 0$ and therefore τ_{k+1} is identically zero. In this particular example with the free projection forecast, the projected Moreau scheme (28) is equivalent to the original one.

In the case of the bouncing ball, it clearly appears that the projection brings some energy to the system. In Fig. 6, the discrete kinetic energy, potential energy and the total mechanical energy are plotted versus time. Each projection onto the constraints affects the energy balance. At the instants of the projection, an increase of the potential energy is shown. In Fig. 7, the coefficient of restitution is chosen equal to one such that the continuous system

is conservative. We observe an increase of the total amount of energy of the system.

Although the convergence is not rigorously proved in the paper, it does not seem to call into question since the amplitude of the oscillatory artifact goes to zero as the time-step vanishes. The main weakness generated by the chattering is the quality of the approximation for a finite time-step. With a fixed time-step, the bouncing ball example never shows a still equilibrium and the chattering never stops.

Let us give another example in this section where the oscillations prevent to reach a static equilibrium. Let us consider the mechanism described in Fig. 8. The system is composed of a roller of radius R submitted to an external applied torque Γ and a slider of mass m which hits the roller. The contact of the roller and the slider is modeled by the Signorini condition, the Newton impact

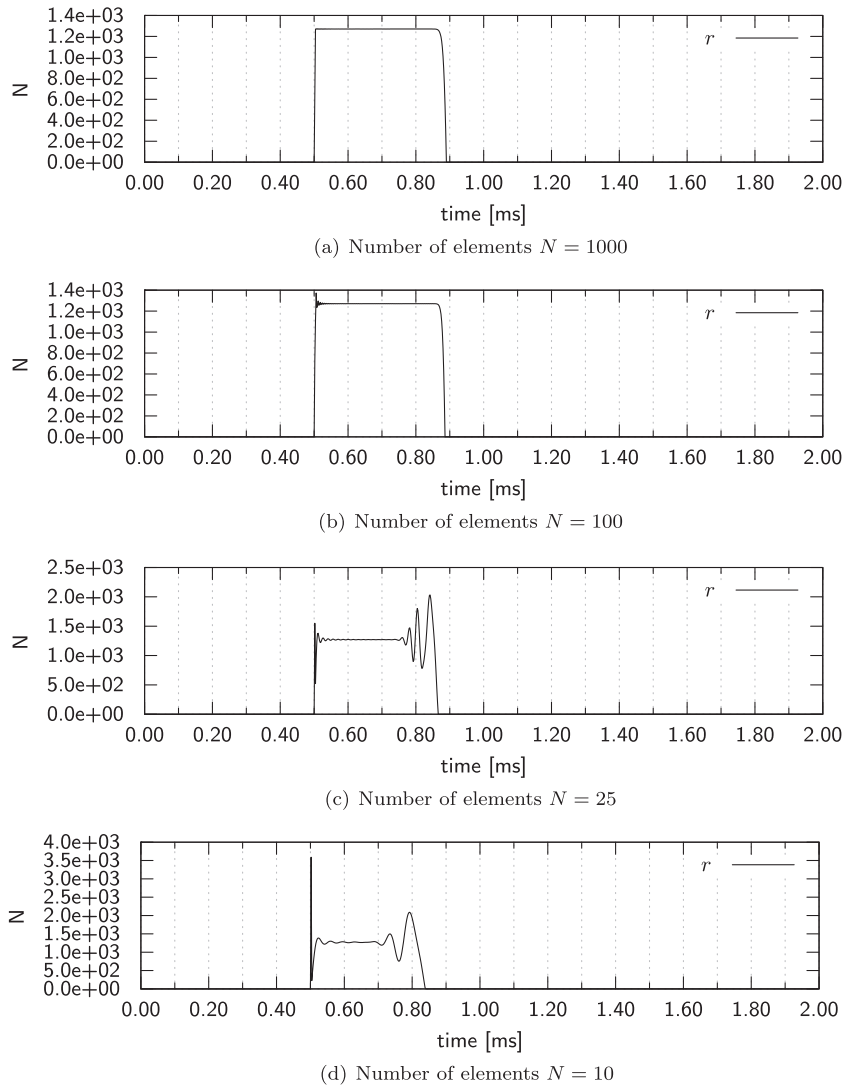


Fig. 13. Contact force r for Moreau–Jean’s scheme. $\theta = 1/2$, $h = 2 \times 10^{-06}$ s. Effect of the element length.

law with a coefficient $e < 1$ and Coulomb’s friction of coefficient μ . The whole system is submitted to gravity. If the applied torque value is less than μmg , a static equilibrium must be reached. If the simulation is achieved with the standard Moreau–Jean scheme, the equilibrium is correctly approximated and observed with a finite time-step. With the direct projected scheme, the slider never stops to bounce and each time the contact is lost, we observe a slip of the roller under the slider. Therefore, the roller never reaches its static equilibrium.

4.6. Conclusion on the direct projected scheme

As often with a time-discretization method which is assumed to be convergent, the approximate solution in discrete-time does not keep all the properties of the continuous time solution. This is the goal of the geometric time-integration methods to ensure the conservation of properties in discrete time [22]. With the direct projected scheme, the constraints in velocity and position are satisfied in discrete time. The algorithm keeps the order of the standard Moreau–Jean scheme and the multiplier associated with the projection vanishes at the order $\mathcal{O}(h)$. With the decoupled approach, the implementation is straightforward and requires only slight modifications of the standard Moreau–Jean scheme.

Table 1

Geometrical and material parameters and initial conditions for the impacting bar example.

Geometrical properties	$L = 1.0$ m
Material properties	$S = 3.14 \times 10^{04}$ m ²
	$\rho = 7800$ kg m ⁻³
	$E = 210$ GPa
Initial conditions	$v_0 = -0.1$ m s ⁻¹

The main drawback is the occurrence of the chattering at contact in some special configurations. The chattering can have major consequences as we can lose in several situations the existence of equilibria. This is not satisfactory for our purpose and the goal of the next section is to remedy to this drawback, retaining the favorable properties of the direct projected scheme.

5. A combined projection/activation algorithm

In this section, we present a scheme to circumvent a part of the problems listed in the previous section. The main goal of this new improved scheme is to activate consistently the constraints at the velocity level with respect to the set of constraints which will be

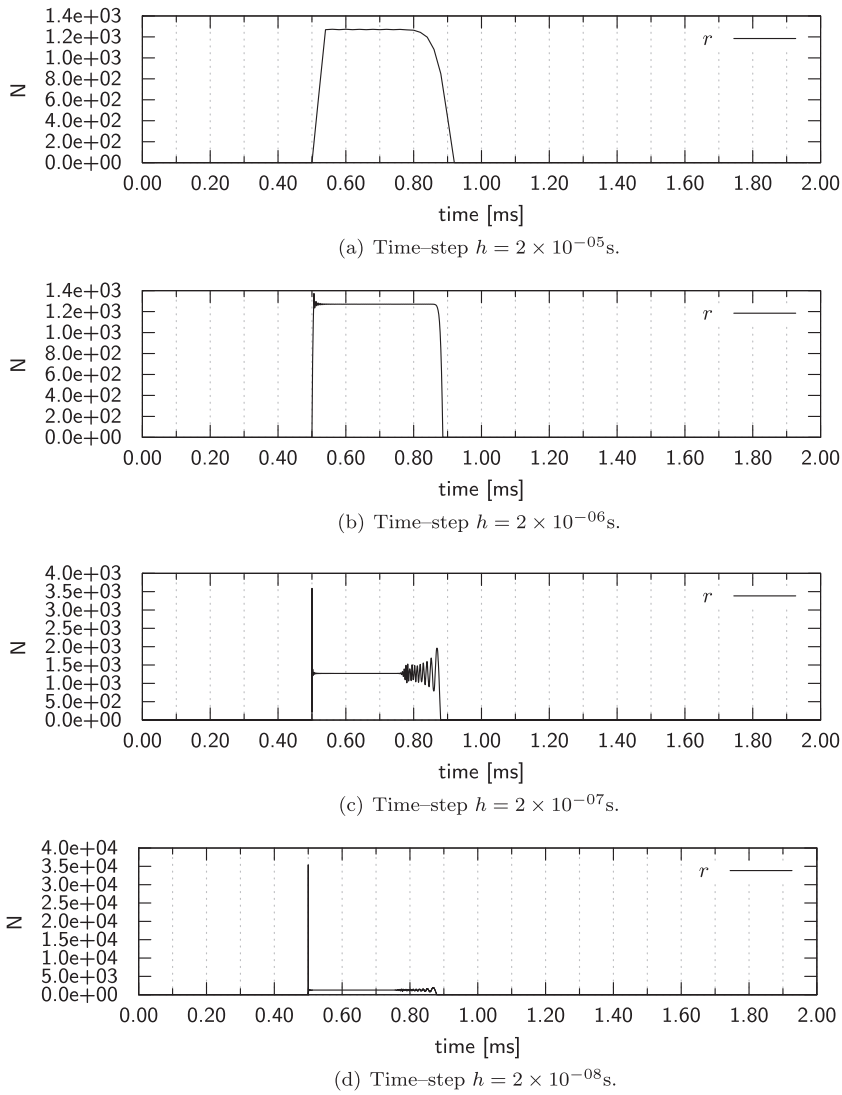


Fig. 14. Contact force r for Moreau–Jean’s scheme. $\theta = 1/2$. Number of elements $N = 100$. Effect of the time-step.

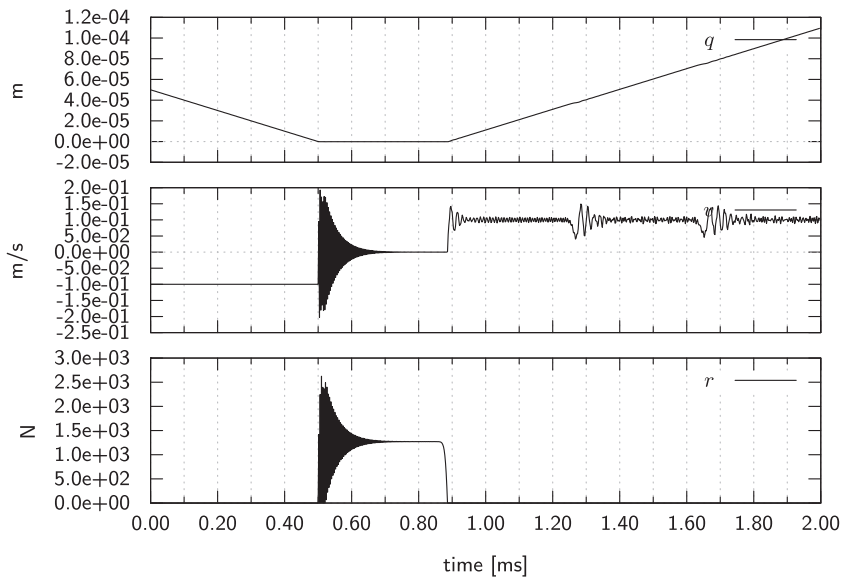


Fig. 15. Moreau–Jean’s scheme with a restitution coefficient $e = 0.95$. $h = 2 \times 10^{-06}$ s. Number of elements $N = 100$.

projected in the current time-step. Especially, we want to avoid the projection onto the constraints if the constraint at the velocity level is not activated. We have seen in Section 4 that these phenomena causes chattering in the direct projection scheme.

5.1. Presentation of the combined scheme

The combined scheme is based on the iterations denoted by ν of the following two steps:

1. The *projection step* is based on the solution of the following system

$$\begin{cases} M(q_{k+\theta})(v_{k+1} - v_k) - hF_{k+\theta} = G(q_{k+1})P_{k+1}, \\ q_{k+1} = q_k + hv_{k+\theta} + G(q_{k+1})\tau_{k+1}, \\ U_{k+1} = G^\top(q_{k+1})v_{k+1}, \\ g_{k+1} = g(q_{k+1}), \\ \text{for all } \alpha \in \mathcal{I}^v \begin{cases} 0 \leq U_{k+1}^\alpha + eU_k^\alpha \perp P_{k+1}^\alpha \geq 0, \\ g_{k+1}^\alpha = 0, \tau_{k+1}^\alpha, \text{ if } P_{k+1}^\alpha > 0, \\ 0 \leq g_{k+1}^\alpha \perp \tau_{k+1}^\alpha \geq 0 \text{ otherwise,} \end{cases} \end{cases} \quad (65)$$

for a given index set \mathcal{I}^v of active constraints.

2. The *activation step* computes the index set \mathcal{I}^v of active constraints by checking for a given value of g_{k+1} if the constraint is satisfied or not. Starting from $\mathcal{I}^0 = \emptyset$, at each iteration ν , the activation performs the following operation

$$\mathcal{I}^{\nu+1} = \mathcal{I}^\nu \cup \{\alpha | g_{k+1}^\alpha \leq 0\}. \quad (66)$$

The iterates of the solution q_{k+1} , v_{k+1} depends on the iteration number ν . In order to avoid useless complexity in the notation, we skip the superscript ν when there is no ambiguity. With this convention, the algorithm is described in Algorithm 2.

Algorithm 2. Activation/Projection Algorithm for one time-step.

Require: h time-step, $l = [t_k, t_{k+1}]$

Require: q_k, v_k initial conditions of the step.

Ensure: $q_{k+1}, v_{k+1}, P_{k+1}, \tau_{k+1}$

// Initialization

$\nu \leftarrow 0$

$\mathcal{I}^0 \leftarrow \emptyset, \mathcal{I}^{-1} \leftarrow \{-1\}$

while $\mathcal{I}^\nu \neq \mathcal{I}^{\nu-1}$ **do**

// Solve the projection step (Eq. (65)).

$$\begin{cases} M(q_{k+\theta})(v_{k+1} - v_k) - hF_{k+\theta} = G(q_{k+1})P_{k+1}, \\ q_{k+1} = q_k + hv_{k+\theta} + G(q_{k+1})\tau_{k+1}, \\ U_{k+1} = G^\top(q_{k+1})v_{k+1}, \\ g_{k+1} = g(q_{k+1}), \\ \text{for all } \alpha \in \mathcal{I}^v \begin{cases} 0 \leq U_{k+1}^\alpha + eU_k^\alpha \perp P_{k+1}^\alpha \geq 0, \\ g_{k+1}^\alpha = 0, \tau_{k+1}^\alpha, \text{ if } P_{k+1}^\alpha > 0, \\ 0 \leq g_{k+1}^\alpha \perp \tau_{k+1}^\alpha \geq 0 \text{ otherwise.} \end{cases} \end{cases}$$

// Update the index set (Eq. (66))

$\mathcal{I}^{\nu+1} \leftarrow \mathcal{I}^\nu \cup \{\alpha | g_{k+1}^\alpha \leq 0\}$

$\nu \leftarrow \nu + 1$

end while

5.2. Comments

Let us first note that the results in Propositions 1 and 2 are still valid for this combined projection/activation scheme.

The first step (65) is very similar to the scheme presented in Section 4. Note that only the index set onto we project is modified. This *a priori* minor modification in the implementation is nevertheless crucial for the qualitative behavior of the scheme.

Let us give now some insight on the behavior of the scheme. The first iteration is performed with $\mathcal{I}_0 = \emptyset$, which amounts to computing the free velocity and the free position of the system. The goal is to perform the first activation of the constraints. In other terms we first perform a step disregarding the constraints and we check what are the constraints which are not satisfied. The indices of these constraints that are violated compose the set \mathcal{I}_1 , that is the first set of forecast activated constraints.

Let us introduce a new index set \mathcal{I}_c^v , subset of \mathcal{I}^v , i.e. $\mathcal{I}_c^v \subset \mathcal{I}^v$ such that

$$\mathcal{I}_c^v = \{\alpha \in \mathcal{I}^v | P_{k+1}^\alpha > 0\}. \quad (67)$$

In the projection step, the following rule is used for the projection

$$\text{for all } \alpha \in \mathcal{I}^v \begin{cases} 0 \leq U_{k+1}^\alpha + eU_k^\alpha \perp P_{k+1}^\alpha \geq 0, \\ g_{k+1}^\alpha = 0, \tau_{k+1}^\alpha, \text{ if } \alpha \in \mathcal{I}_c^v, \\ 0 \leq g_{k+1}^\alpha \perp \tau_{k+1}^\alpha \geq 0 \text{ otherwise.} \end{cases} \quad (68)$$

We note that the projection is only performed for the active constraints whose index belong to \mathcal{I}_c^v (positive contact impulse $P_{k+1}^\alpha > 0$). For the constraints $\alpha \in \mathcal{I}^v \setminus \mathcal{I}_c^v$, we project onto the manifold defined by $\{g_{k+1}^\alpha = 0, \alpha \in \mathcal{I}_c^v\}$. Otherwise, we only require to have non-penetration. Even if there is no rigorous mathematical proof, this correction rule reveals as the best compromise in practice. Indeed, imposing $g_{k+1}^\alpha = 0$ for all constraints in \mathcal{I}^v may lead to unfeasible problem. At the end of the time step, we ensure that there are no violated constraint and no projected constraint without satisfying the jump rule $0 \leq U_{k+1}^\alpha + eU_k^\alpha \perp P_{k+1}^\alpha \geq 0$.

Concerning the implementation, the projection step is very similar to the direct projection scheme presented in Section 4. Its implementation follows the same line as in Section 4.3. It can be decoupled or not. As for the evaluation of \mathcal{I}^v , we need to precise the rule for the computation of \mathcal{I}_c^v in order to obtain a proper LCP without switched-off constraints triggered by a conditional statement. The rule that we have chosen is

$$\mathcal{I}_c^v = \{\alpha \in \mathcal{I}^v | P_{k+1}^{\alpha} > 0\} \quad (69)$$

for a coupled scheme and

$$\mathcal{I}_c^v = \{\alpha \in \mathcal{I}^v | P_{k+1}^{\alpha} > 0\} \quad (70)$$

for the decoupled scheme since we known the value of $P^{\nu+1}$ from the solution of the first LCP.

5.3. Rocking block example

The efficiency of Algorithm 2 is firstly demonstrated on the rocking block (Example 3). In terms of spurious oscillations, the others academic examples are simpler to deal with. Since the rocking block example has two strongly coupled nonlinear constraints, we focus our attention in this section on it. More complex examples will be treated in Section 6.

In Fig. 9, the results of the scheme based on a direct projection in Algorithm 1 is compared with Algorithm 2 based on the combination of projection and activation steps. The simulation parameters are as follows: $l = 1.5$ m, $L = 1$ m, $x_0 = 0.0$ m, $y_0 = 1.0$ m, $\theta_0 = 0.2$ rad, $\dot{x}_0 = 0.0$ m s⁻¹, $\dot{y}_0 = 0.0$ rmm s⁻¹, $\dot{\theta}_0 = 0.2$ rad s⁻¹, $m = 1.0$ rmmkg, $e = 0.5$, $t_0 = 0.0$ s, $T = 2.0$ s, $h = 10^{-02}$ s, $\theta = 1/2$. In Fig. 9(c), the spurious oscillations are observed when the rocking block reaches its equilibrium after a finite accumulation of impacts. In Fig. 9(d), we remark that the spurious oscillations are suppressed and the block reaches its equilibrium without any troubles. On the energetic point of view (Fig. 9(e) and (f)), the combined

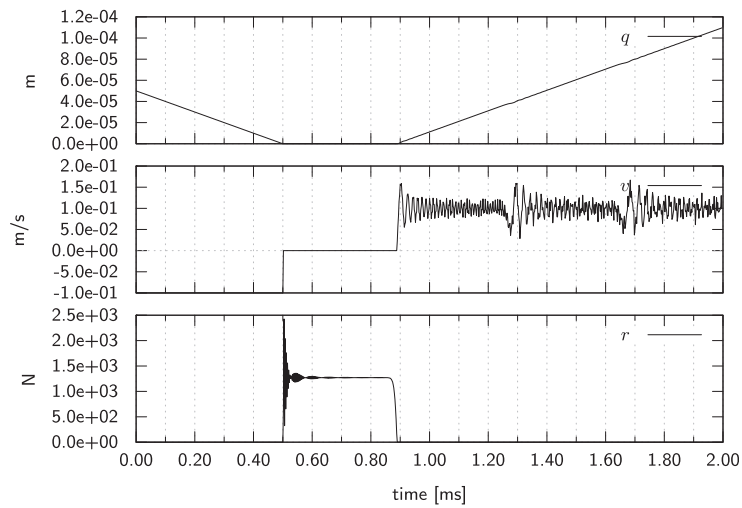


Fig. 16. Combined scheme (Algorithm 2). Position q , velocity v and reaction force r at the contact point. $\theta = 1/2$, $h = 2 \times 10^{-6}$ s. Number of elements $N = 1000$.

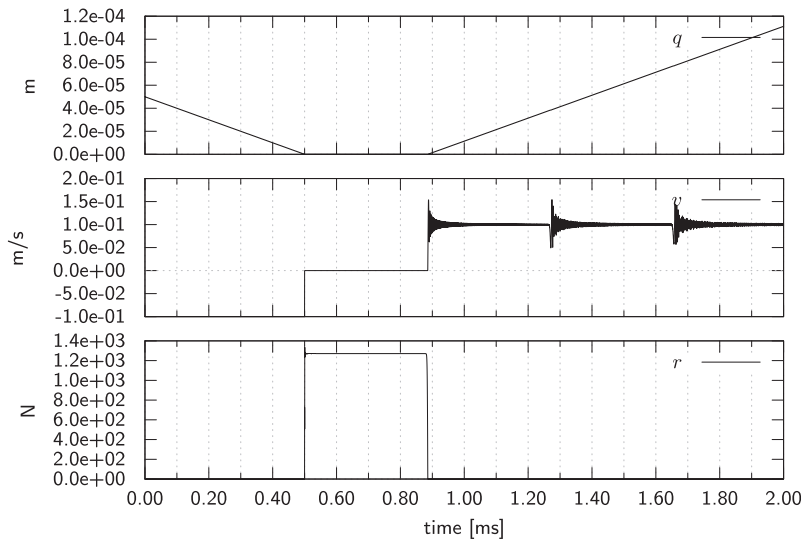


Fig. 17. Combined scheme (Algorithm 2). Position q , velocity v and reaction force r at the contact point. $\theta = 1/2$, $h = 2 \times 10^{-7}$ s. Number of elements $N = 1000$.

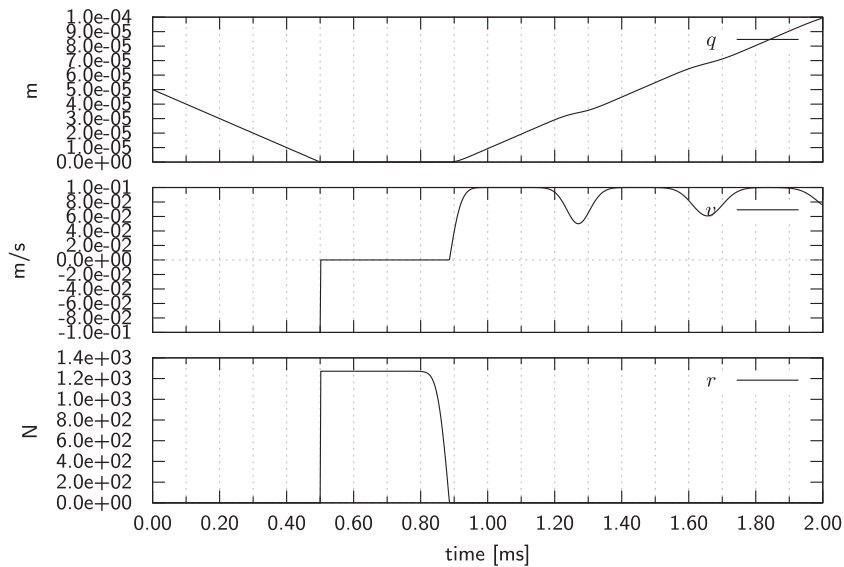


Fig. 18. Combined scheme (Algorithm 2). Position q , velocity v and reaction force r at the contact point. $\theta = 1$, $h = 2 \times 10^{-7}$ s. Number of elements $N = 1000$.

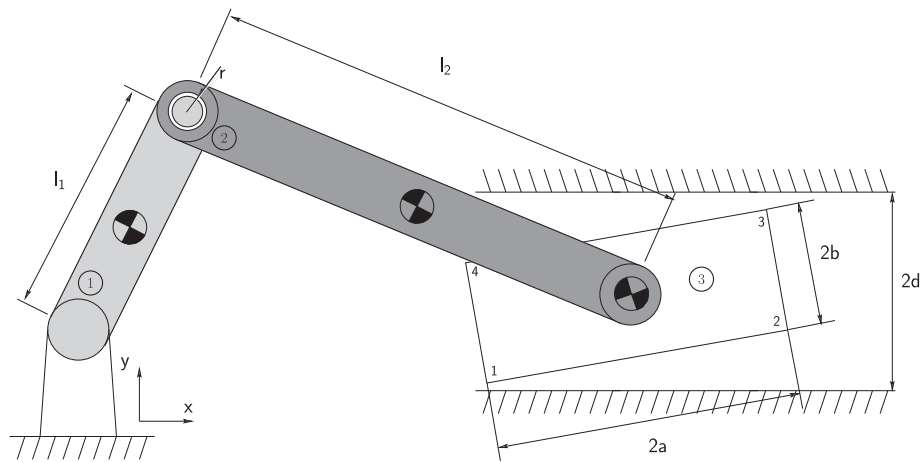


Fig. 19. Classical slider-crank mechanism with clearances: (1) the crank, (2) the connecting rod and (3) the slider. Clearances in the translational joint and in the revolute joint between the crank and the connecting rod.

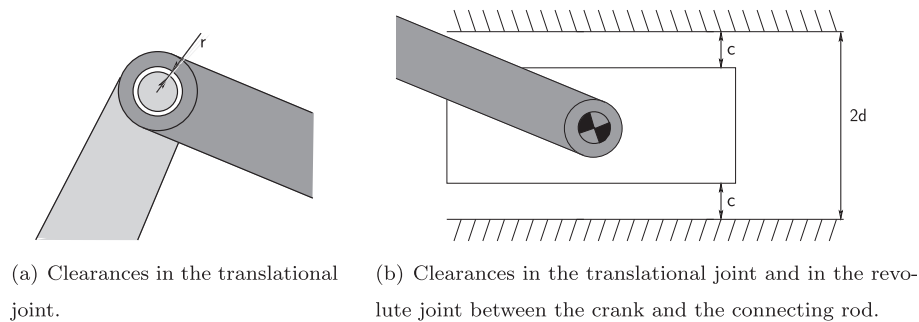


Fig. 20. Details of the clearance modeling.

approach dissipates more energy than the standard direct approach. With the requirement that the time-step length does not depend on events, dissipation of energy is the price to pay to avoid chattering with a projection onto the constraints.

6. Demonstrative applications

6.1. Software aspects

Algorithms 1 and 2 are implemented in the open-source SICONOS software [6,51]. This software provides a general framework for implementing numerical time integration schemes of nonsmooth dynamical systems. The solver for the discrete frictional contact problem that is used in this paper is a projected Gauss-Seidel solver [28] developed in the SICONOS/NUMERICS library of solvers. In the most of the following examples, the SICONOS/MULTIBODY library is used to model and simulate multibody systems with three-dimensional contact, impacts and Coulomb's friction. This library allows the user to instantiate a Newton/Euler model linked to a geometrical representation in a industrial CAD library. In our examples, we use the open-source Software CAD library OPENCASCADE [57] and its python wrapper PYTHONOCC [43].

6.2. The impacting elastic bar

The example which is considered in this section is the problem of a one-dimensional bar which hits a rigid wall with a constant initial velocity v_0 . We assume that the assumption of small displacements holds and the constitutive law is linear elastic. The problem depicted in Fig. 10 consists of a linear elastic bar of cross

Table 2

Geometrical, mechanical and numerical parameters used in the slider-crank model.

Geometrical properties	$l_1 = 0.1530$ m $l_2 = 0.3060$ m $a = 0.0500$ m $b = 0.0250$ m $c = 0.0010$ m $d = 0.0520$ m
Inertial properties	$m_1 = 0.0380$ kg $m_2 = 0.0380$ kg $m_3 = 0.0760$ kg $J_{y,1} = J_{z,1} = 7.4 \times 10^{-5}$ kg m ² $J_{x,1} = 1 \times 10^{-5}$ kg m ² $J_{y,2} = J_{z,2} = 8.9 \times 10^{-4}$ kg m ² $J_{x,2} = 1 \times 10^{-5}$ kg m ² $J_{y,3} = J_{z,3} = 2.7 \times 10^{-6}$ kg m ² $J_{x,2} = 1 \times 10^{-5}$ kg m ²
Contact parameters	$e = 0.4$, $\mu = 0.01$ (slider/cylinder contact) $e = 0.0$, $\mu = 0.01$ (crank/connecting rod joint)
Numerical parameters	$\theta = 1/2$, Newton tolerance 10^{-10} , violation tolerance 10^{-10}

section area S , with a Young modulus E and density ρ and of length L . This problem has been widely used in the literature (see for instance [24,23,58]) because of its interest from the mathematical and computational point of view.

From the mathematical point of view, this example is one of the rare example in elastodynamics with unilateral contact for which the mathematical properties are known in terms of existence and uniqueness. The problem of an elastic bar is indeed discussed from

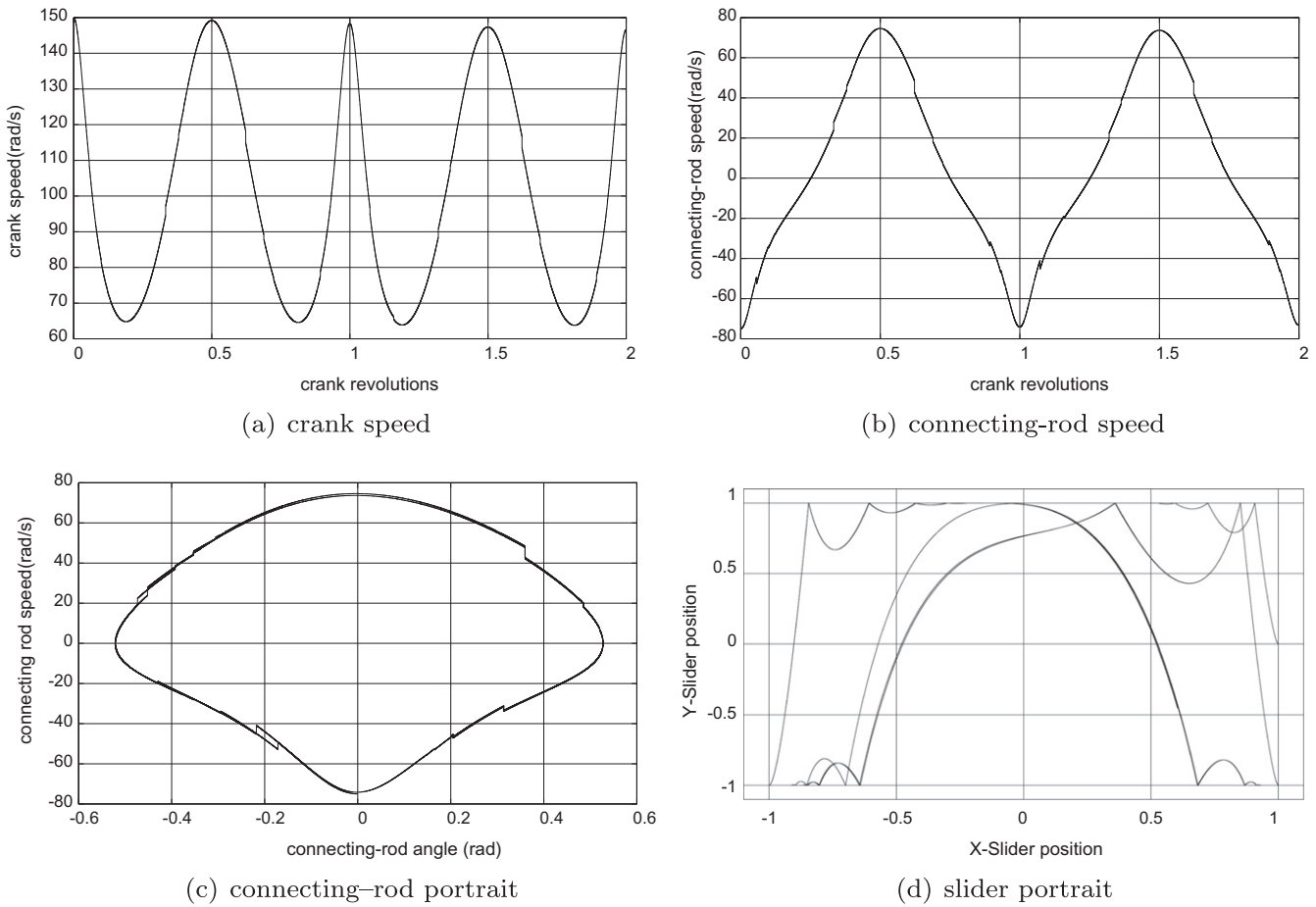


Fig. 21. Details of the motion of the slider-crank with the standard Moreau–Jean time-stepping scheme for $h = 10^{-6}$ s.

Table 3
Details on the computational efficiency of the projection algorithms in the Lagrangian setting.

Method	Time-step [s]	Violation [m](max.)	Newton iteration (avg./max.)	Projection iteration (avg./max.)	Index sets iteration (avg./max.)
Moreau–Jean (18d)	10^{-04}	1.324×10^{-04}	2.95/4	N/A	N/A
Moreau–Jean (18d)	10^{-05}	1.234×10^{-05}	1.99/3	N/A	N/A
Moreau–Jean (18d)	10^{-06}	1.119×10^{-06}	1.96/2	N/A	N/A
Algorithm 1	10^{-04}	8.099×10^{-11}	1.96/2	0.09/2	N/A
Algorithm 1	10^{-05}	4.833×10^{-11}	1.01/2	0.11/1	N/A
Algorithm 1	10^{-06}	9.99×10^{-11}	1.001/2	0.04/1	N/A
Algorithm 2	10^{-04}	8.410×10^{-11}	2.15/4	0.20/2	1.18/2
Algorithm 2	10^{-05}	9.940×10^{-11}	1.127/2	0.019/1	1.127/2
Algorithm 2	10^{-06}	8.650×10^{-11}	1.12/2	0.00036/1	1.12/2

the mathematical point of view in [49] with an associated numerical scheme. It is shown that the problem can be uniquely solved without requiring any additional energetic condition. More general cases are complex. The vibration of a string on a point-shaped obstacle enjoys also existence and uniqueness. It has been proven in [48] without asking for an additional energy condition. For a concave continuous obstacle, an energy condition has to be added to retrieve uniqueness (see [47]). For more complex geometries, the problem remains open. For the elastic impacting bar without external forces, a simple solution can be constructed as in [15]. Let us denote by $c_0 = \sqrt{E/\rho}$ the wave speed. The contact time denoted by T corresponds to twice the time of the traveling of the elastic wave in the bar, that is $T = 2L/c_0$. Within the contact time, the contact force is constant and equal to $r = ESv_0/c_0$.

From the computational point of view, the problem of an impacting elastic bar has also another special interest: it exhibits spurious oscillations of the contact velocity and the contact force when using standard numerical schemes (Newmark, HHT, α -schemes) for elastodynamics. This spurious oscillations which are very different in nature with the chattering observed with the direct projected scheme can be explained at least by two causes. The first one is the nonsmoothness of the solutions. When the tip of the bar reaches the wall, a jump in the velocity of the tip and in the contact forces occurs. If the scheme approximates these unknowns with a second-order approximation, oscillatory artifacts can be observed [33,14,15]. Most of the time, this first cause is circumvented by using a first-order fully implicit treatment of the contact forces [11,32,33], or a direct use of the impulse [35,27].

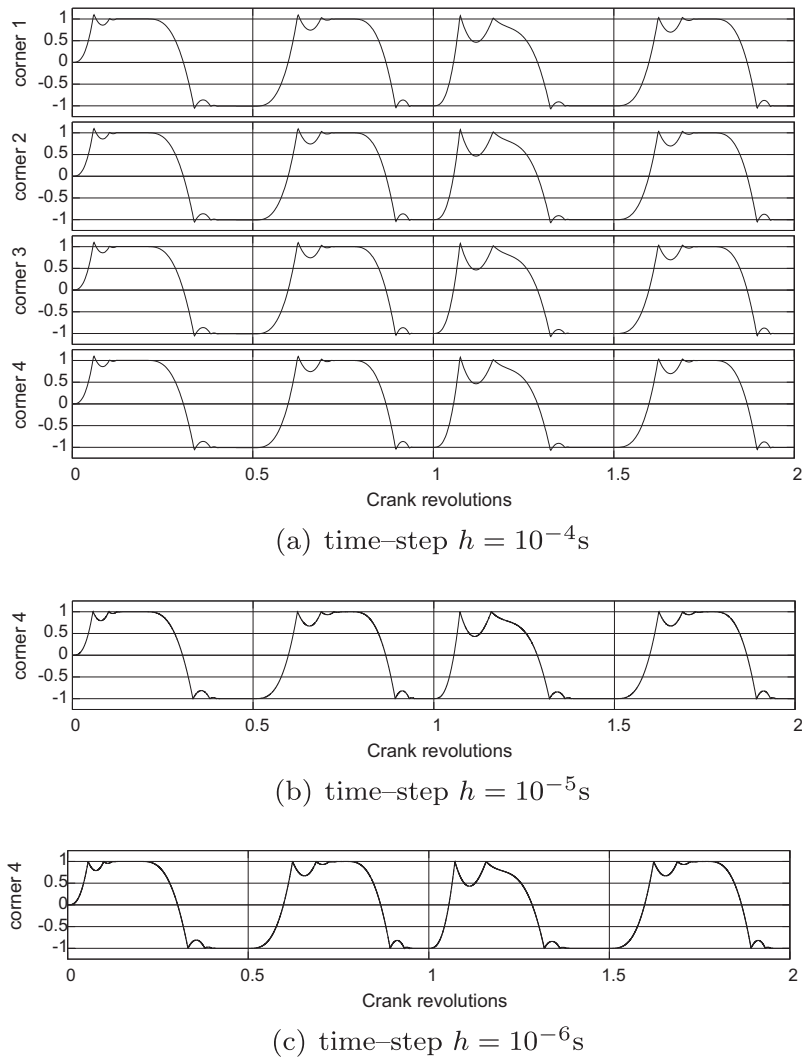


Fig. 22. Dimensionless motion of the slider corners with the standard Moreau-Jean time-stepping scheme for different time-steps.

The second cause of oscillations is the index of the DAE resulting after a time and space discretization. If the unilateral constraint is written at the position level, the index of the DAE for a closed contact is 3. It is well known that the direct time-integration of DAEs of index 3 generates spurious oscillations in the time derivative of the constraints. To remove this oscillation, some attempts have been based on (a) writing of the constraints at the velocity level [31], that is to perform an index reduction similarly as in the Moreau-Jean scheme, (b) redistributing the mass which consists in removing the mass from the contact boundaries [29,30] or (c) stabilizing the relative velocities at contact [14].

In this article, we propose to solve the impacting elastic bar problem by using an index reduction technique with a stabilization of the constraint based on a projection as in the seminal work of Gear et al. [18]. The constraint is written at the velocity level and the dynamics is time integrated with the help of the Moreau-Jean scheme. Using an index reduced formulation at velocity level avoids the spurious oscillations at contact of the forces and the relative velocity. By the way, since the structure is space-discretized, it appears as a finite-freedom mechanical system with unilateral contact for which we know that we have to provide an energy condition under the form of an impact law. We choose a perfect inelastic impact law to mimic the continuous time solution where the contact stays closed for a finite time interval. In more complex

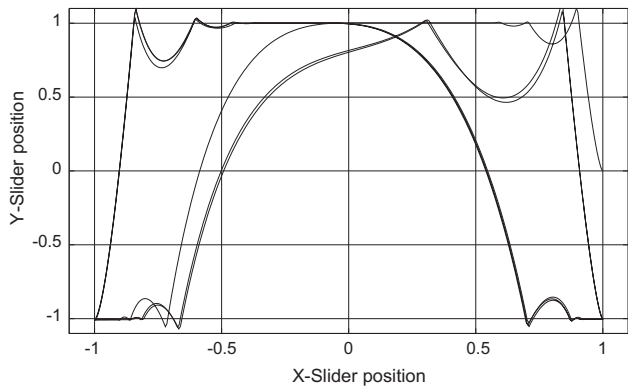
situations, this question remains open. The price to pay in using a velocity based formulation for the constraint is the drift the constraints at the position level. This drift, or violation of the constraints is fixed by the projection onto the constraints and the additional multiplier.

In the results that follow, the bar is space discretized by N linear rod finite elements. The elementary mass and stiffness matrices are

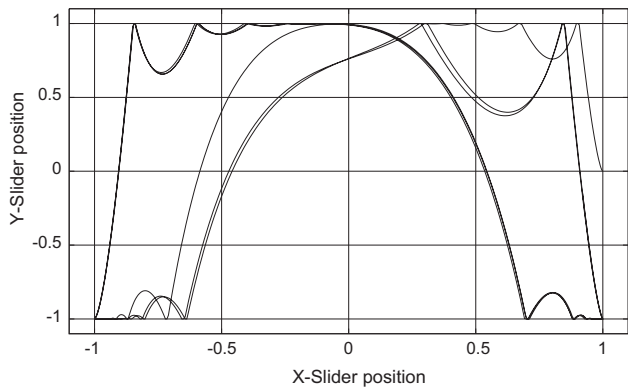
$$M_e = \frac{1}{6} \rho S l_e \begin{bmatrix} 2 & 1 \\ 1 & 2 \end{bmatrix}, \quad K_e = \frac{1}{l_e} ES \begin{bmatrix} 1 & -1 \\ -1 & 1 \end{bmatrix}, \quad (71)$$

where $l_e = L/N$ is the length of an element. The material parameters are summarized in Table 1.

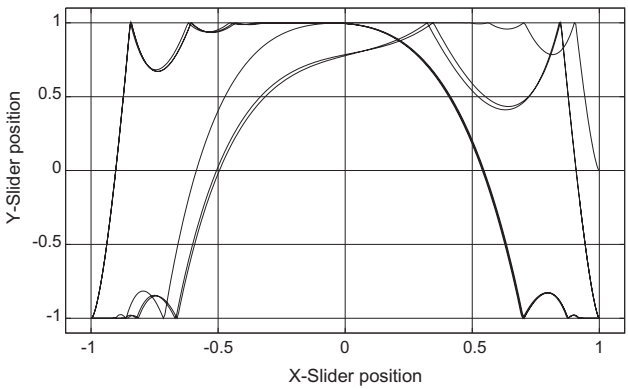
In Fig. 11, the spurious oscillations of the contact velocity and the contact force are depicted for the trapezoidal rule with a contact condition at the position level and an implicit treatment of the contact force. The scheme is similar to the Moreau-Jean scheme with $\theta = 1/2$, but with a position level constraint. Although the constraint at the position level is perfectly satisfied on the time of contact equal to $T = 3.8545 \times 10^{-04}$ s, we note that the contact velocity oscillates between two extreme values at each time step. The oscillations of the contact forces are also observed around the solution value $r = 1271.472$ N. Note that spurious oscillations are also observed for the contact velocity after the contact time, around the solution value $-v_0$. This is mainly due to the jump of



(a) slider portrait with Moreau–Jean’s scheme (18d)



(b) slider portrait with the direct projected scheme. Algorithm 1



(c) slider portrait with the combined scheme. Algorithm 2

Fig. 23. Slider portrait for $h = 10^{-04}$ s with different time-stepping schemes.

the contact force that excites the artificial high frequency modes of the bar induced by the space discretization. Using the pure trapezoidal rule does not enable us to introduce a small amount of numerical dissipation which would allow us to damp these latter oscillations.

With the Moreau–Jean scheme, the spurious oscillations within the contact time are not observed in Fig. 12. The constraint at the velocity level with a coefficient of restitution $e = 0$ yields a perfect stabilization of the velocity. The post contact oscillations due to the high-frequencies modes are still observed due to the lack of numerical damping. A very small oscillation of the contact force

occurs in the first step after the bar reaches the obstacle can be also observed. It is mainly due to the fact that we deal with a finite-freedom system and the flexible structure is subjected to an impact. In order to understand a little bit further this phenomenon, Figs. 13 and 14 provide us with an analysis of the contact force with respect to the element size and the time-step. In Fig. 13, it appears that for a decreasing number of elements, an increasing peak appears in the contact force. This peak reveals the occurrence of an impact when the bar reaches the obstacle. The peak increases since the finite mass of the last element involved in the contact increases as well. In Fig. 14, we observe that the peak increases with a decreasing time-step for a constant number of elements. In the limit, we may expect that the value of this peak goes to infinity which is another expression of the occurrence of an impact. For a vanishing time-step and a fixed mesh size, we converge to the behavior of a finite-freedom mechanical system with impact and the contact force goes to infinity. The right unknown is then the impulse. As we said earlier, the presence of an impact and an impulse calls for the introduction of an impact law. In this simple case, we know *a priori* that the bar should be in closed contact for a finite-time interval. This is the reason why we choose a Newton impact law with a coefficient of restitution equal to 0. In Fig. 15, we report the results of the same scheme with $e = 0.95$. Since the discretized model is a finite-freedom mechanical system, the choice of a coefficient of restitution in $[0, 1]$ yields a well-posed problem. However, in the limit when the mesh size vanishes, we cannot expect to retrieve the elastic bar problem as the oscillations of the contact velocity shows.

This section is completed with the application of the combined projected scheme to the elastic bar example. In the previous example, the violation of the constraints ranges from 2.5×10^{-05} m to 2.5×10^{-08} m for a time-step from $h = 5 \times 10^{-05}$ s to $h = 5 \times 10^{-07}$ s. When the projected scheme is applied, the violation is equal to zero at the machine accuracy. In Figs. 16 and 17, the bar tip position and velocity are depicted. They are very similar to those obtained with the Moreau–Jean scheme. For the contact force, spurious oscillations are observed due to the jump in position that excites the high-frequency modes of the structure. Nevertheless, and contrary to the real impact at the velocity level, these oscillations vanish as the time-step decreases, since the projection multiplier also vanishes. To conclude, we are able, for a flexible structure, to satisfy at the same time the constraints in position and in velocity. The high-frequency mode excitation of the structure calls for the introduction of numerical damping. These can be achieved by using $1 \geq \theta \gg 1/2$ as it is illustrated in Fig. 18. Nevertheless, the use of numerical damping with the θ -method implies a dissipation over the whole range of frequencies. As we can observe, the response of the structure is roughly damped. In [12], a consistent adaptation of the HHT scheme and the α -schemes to the impact mechanics is proposed to this end. The adaptation of the projected approach could be a solution in this framework.

6.3. Classical slider–crank mechanism

In this section, we are interested in the application of the proposed schemes to a classical mechanism: the slider–crank. The slider crank mechanism depicted in Fig. 19 is composed of three mobile bodies: the crank (\odot ; in light gray), the connecting rod (\ominus ; in dark gray) and the slider (\odot ; in white). Concerning the clearances in joints, two configurations will be studied. In the first one, there is only play in the transitional joint between the slider and the cylinder. In the second configuration, a play is also introduced in the revolute joint between the crank and the connecting rod. In each configuration, the clearance is modeled by a unilateral contact with Coulomb’s friction and Newton’s impact law. The modeling of

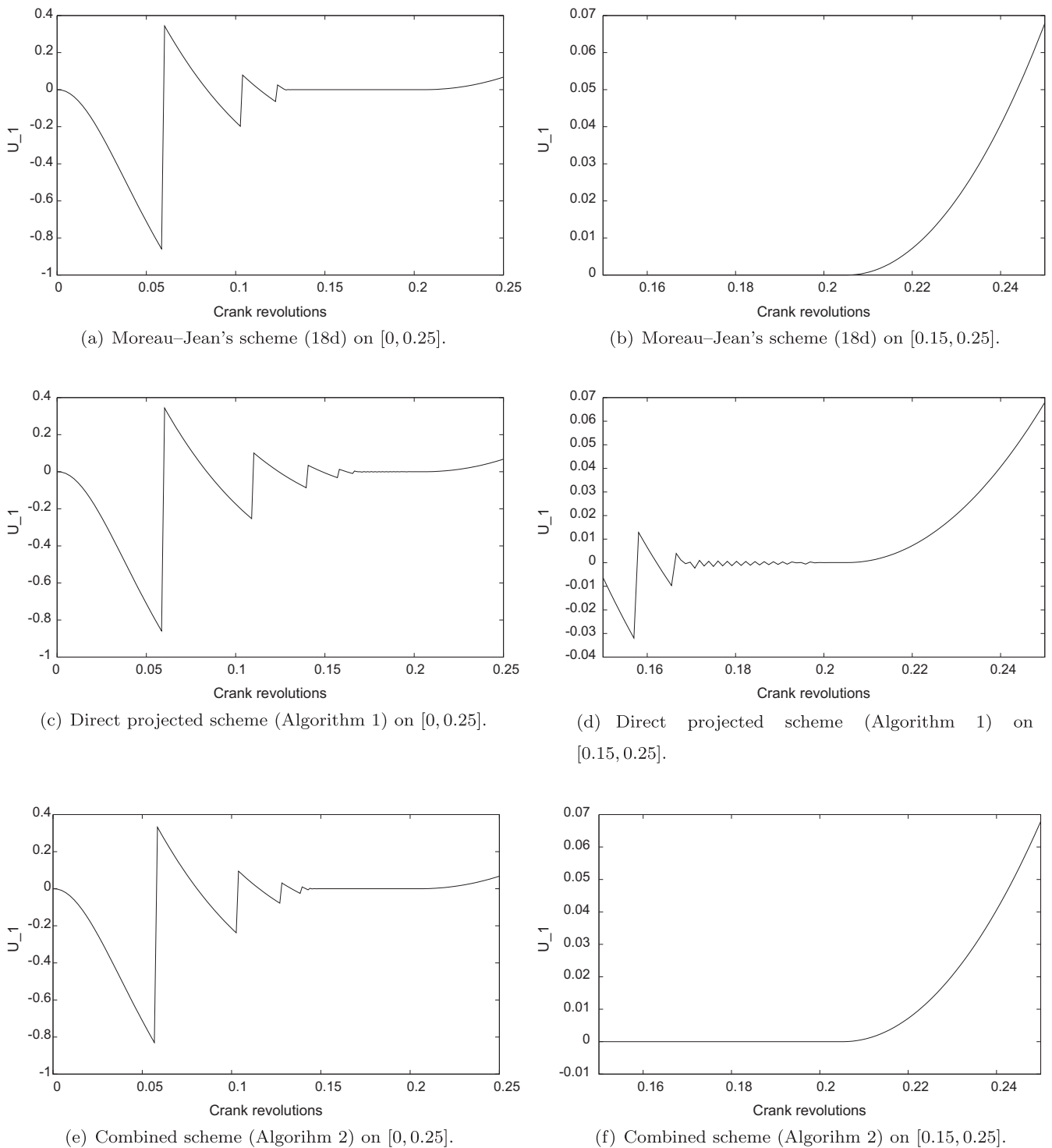


Fig. 24. Details on the relative velocity vs. the crank revolution at corner 1 with different time-stepping schemes. $h = 10^{-4}$ s.

clearances is detailed in Fig. 20. The size of the play between the crank and the connecting rod is denoted as r .

In the sequel, we will consider that the first configuration is obtained with a zero play, i.e., $r = 0$. This configuration is identical to those developed in [17] where the slider–crank is studied in the nonsmooth dynamics framework with a model based on unilateral contact, Coulomb’s friction and Newton’s impact law. The time integration in [17] is performed with the Moreau–Jean time-stepping scheme. In a first step (Section 6.3.1), the equations of motion and the unilateral constraints are written in a pure Lagrangian

setting with minimal coordinates chosen as in [17]: the generalized coordinates is defined by the crank angle, the connecting rod angle and the slider angle with respect to the x -axis. In a second step (Section 6.3.2), we use the full Newton/Euler formalism with maximal coordinates to facilitate the introduction of clearances in every joint of the mechanism.

In order to validate our approach and our model, the geometrical and mechanical properties for the system are rigorously the same as in [17]. They are listed in Table 2. The main discrepancy with [17] is the adaptation of the geometry for the full

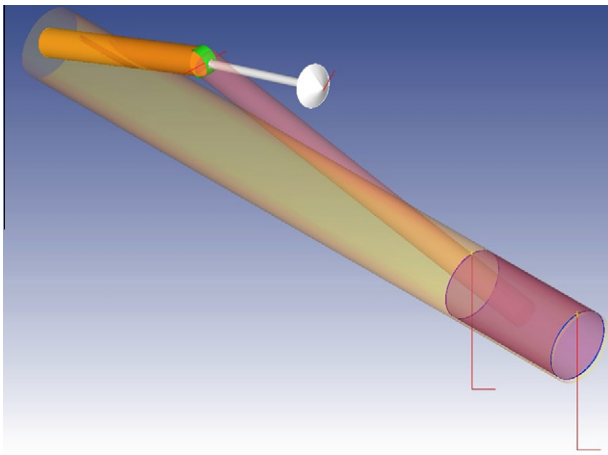


Fig. 25. CAD view of the slider-crank mechanism using OPENCASCADE [57] and PYTHONOCC [43].

three-dimensional case in Section 6.3.2: the crank, the connecting rod and the slider are considered to be slender rods rather than planar laminates (see Fig. 25 for an illustration). In their initial positions, the cylinders are aligned with the x -axis and the moments of inertia in Table 2 are given along their principal axis of inertia which coincides with the (x, y, z) frame at the initial time.

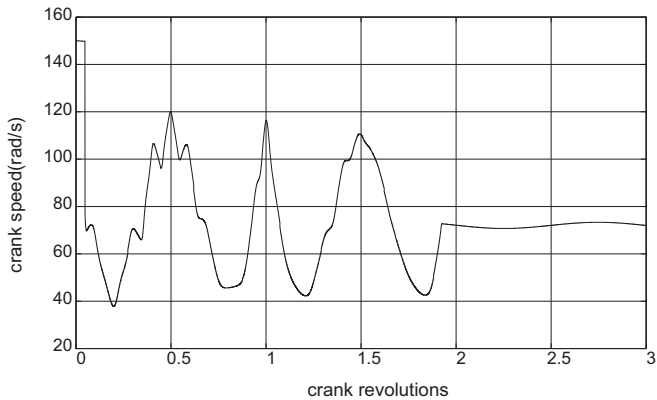
The system is under the action of the gravity acceleration equal to $g = 9.81 \text{ m s}^{-2}$. The initial conditions are also chosen as in [17]: the slider-crank is aligned with the x -axis and initial angular

velocities are imposed to the crank ($\omega_{1,z} = 150 \text{ rad/s}$) and the connecting rod ($\omega_{2,z} = -75 \text{ rad/s}$).

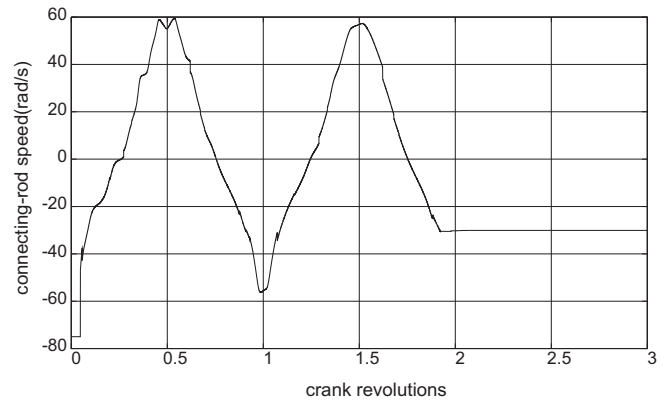
6.3.1. Lagrangian setting with no clearance between the crank and the connecting rod

As we recalled earlier in this section, we use the pure Lagrangian setting with minimal coordinates and without any play in the revolute joint. In Fig. 21, the results of the simulation with the classical Moreau-Jean scheme are reproduced for the time-step $h = 2 \times 10^{-6}$ over two crank revolutions. The results corroborate those in [17]. In Fig. 22, the motion of the corners of the slider are depicted. Note that the motion of the four corners are identical, due to the fact that the contact forces result in a vanishing torque at the center mass. The motion of the slider is therefore a pure translation. We note also some violations of the constraints and drifts of the constraints which are proportional to the time-step. This remark is confirmed by the numerical values reported in Table 3 where the maximum of violation of the constraints is of the same order as the time-step. It also corroborates the result of Proposition 1. In order to minimize the violation of constraints, the discrete frictional contact problem is solved at the velocity level with a relative numerical tolerance of 10^{-12} . With a smaller accuracy (a larger tolerance), the symmetry of the problem may be lost and a drift in the slider angle is observed leading to larger drifts in the constraints.

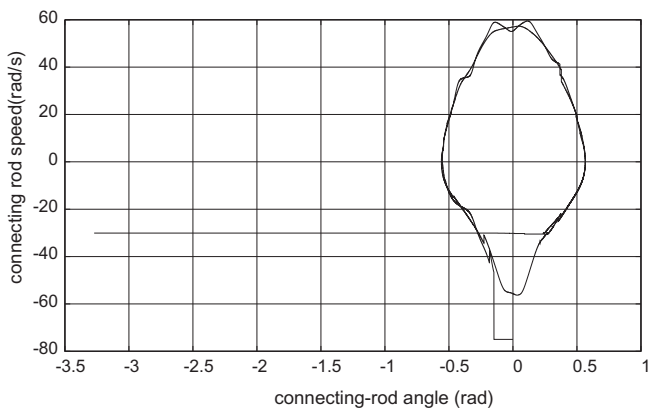
In Fig. 24, the slider portrait (y position with respect to the x position of the slider's center of mass) is depicted for the various schemes: the Moreau-Jean scheme (18d) in Fig. 23(a), the direct projected scheme (Algorithm 1) in Fig. 23(b) and the combined



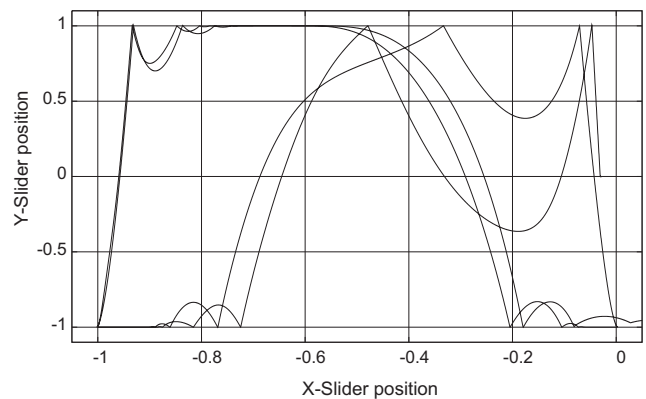
(a) crank speed



(b) connecting-rod speed



(c) connecting-rod portrait



(d) slider portrait

Fig. 26. Details of the motion of the slider-crank with the standard Moreau's time-stepping scheme for $h = 10^{-05} \text{ s}$ and a play in the revolute joint $r = 5 \times 10^{-04} \text{ m}$

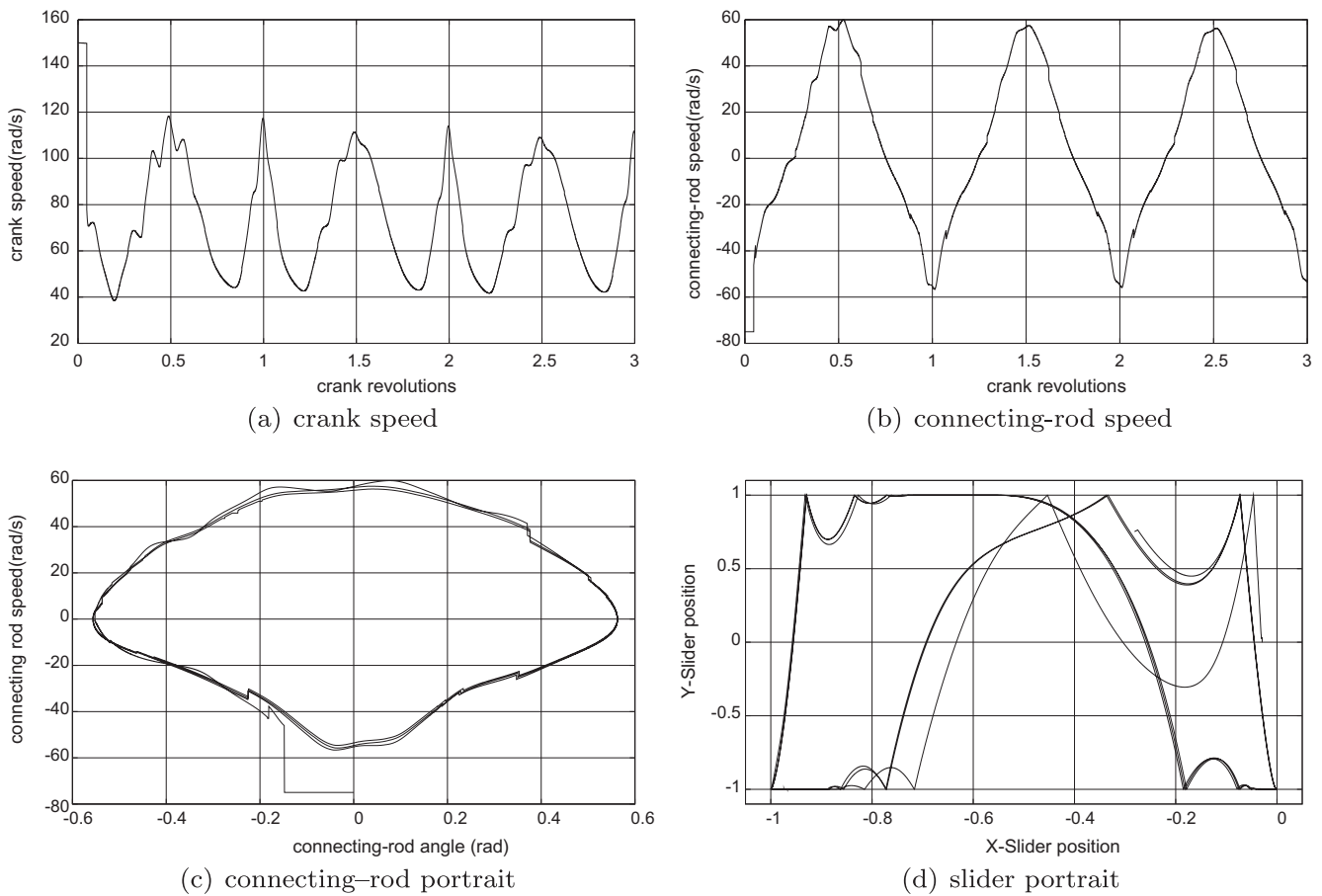


Fig. 27. Details of the motion of the slider crank with the combined projection time-stepping scheme for $h = 10^{-05}$ s and a play in the revolute joint $r = 5 \times 10^{-04}$ m.

scheme (Algorithm 2) in Fig. 23(c). A quite large time-step $h = 10^{-04}$ s is used to exhibit large violations for the Moreau–Jean scheme. These violations can be observed in the kinks of the curve in Fig. 23(a) when the slider’s corners hit the cylinder. In Fig. 23(b) and (c), no more violation of the constraints are observed. It can be checked in Table 3 that the maximum of violations drops from 1.324×10^{-04} to 8.099×10^{-11} by using Algorithm 1. In Fig. 24, we give some details on the relative velocity at the corner 1 of the slider, for values of the crank revolution comprised in $[0, 0.25]$. We can observe in Fig. 24(a) and (b) that the stabilization on the constraints with the Moreau–Jean scheme is smooth. This smoothness is lost with the direct projected scheme as we can observe in Fig. 24(d) some oscillatory artifacts on the relative velocity when the contact should be closed. This is exactly the same phenomenon as we observed in Fig. 4 for the bouncing ball example. In Fig. 24(f), the effect of the combined scheme of Algorithm 2 is to retrieve a smooth stabilization of the constraints by keeping the satisfaction of the constraints at the position level.

In Table 3, we give some details on the computational efficiency of the projected algorithms for various time-steps. The first conclusion that can be drawn on this example is that the number of projection steps is quite low and it does not perturb the convergence of the Newton algorithm. On the contrary, we can observe that the convergence of the Newton algorithm is improved by the projection onto the constraints. We can also observe that the average number of projection iterations with the combined scheme is lower than the average number of iterations for the projected scheme for the time-steps $h = 10^{-05}$ s and $h = 10^{-06}$ s. This is mainly due to the modification of the procedure for activating the constraints. In

the combined scheme, the constraints are most the time activating before the contact is closed.

6.3.2. Newton/Euler setting with clearance between the crank and the connecting rod

In this section, the Newton/Euler equations are used for each body of the mechanism using a maximal set of coordinates (three translations and a unit quaternion to parametrize the finite rotations). The formulation allows us to introduce some clearances in every joint of the mechanism without redefining a new choice of coordinates. In Fig. 25, a view of the CAD is model is given where the arrow represents the reaction force in the revolute joint. The clearance is geometrically modeled by two cylinders that allows out-of-plane motions. With no play in the perfect revolute joint, i.e., the joint is modeled by an ideal revolute joint, the results, which are not reproduced here for a sake of space, perfectly corroborates the curves obtained in [17] and in the previous section (see Figs. 21 and 22).

In Fig. 26, we report the result of the simulation with the standard Moreau–Jean time-stepping scheme with a time-step $h = 10^{-05}$ s. A play of size $r = 5 \times 10^{-04}$ m is introduced in the revolute joint with a perfectly plastic impact law. We can first observe in Fig. 27(a)–(c) that in a first phase, the angular speeds of the crank and the connecting are constant and equal to the prescribed values at the initial time. This reveals that the contact between the crank and the connecting rod is not active up to a first perfectly plastic impact occurs. We can also observe that the presence of clearances in the revolute joint introduces a higher frequency motion around the periodic motion of the slider. Most importantly,

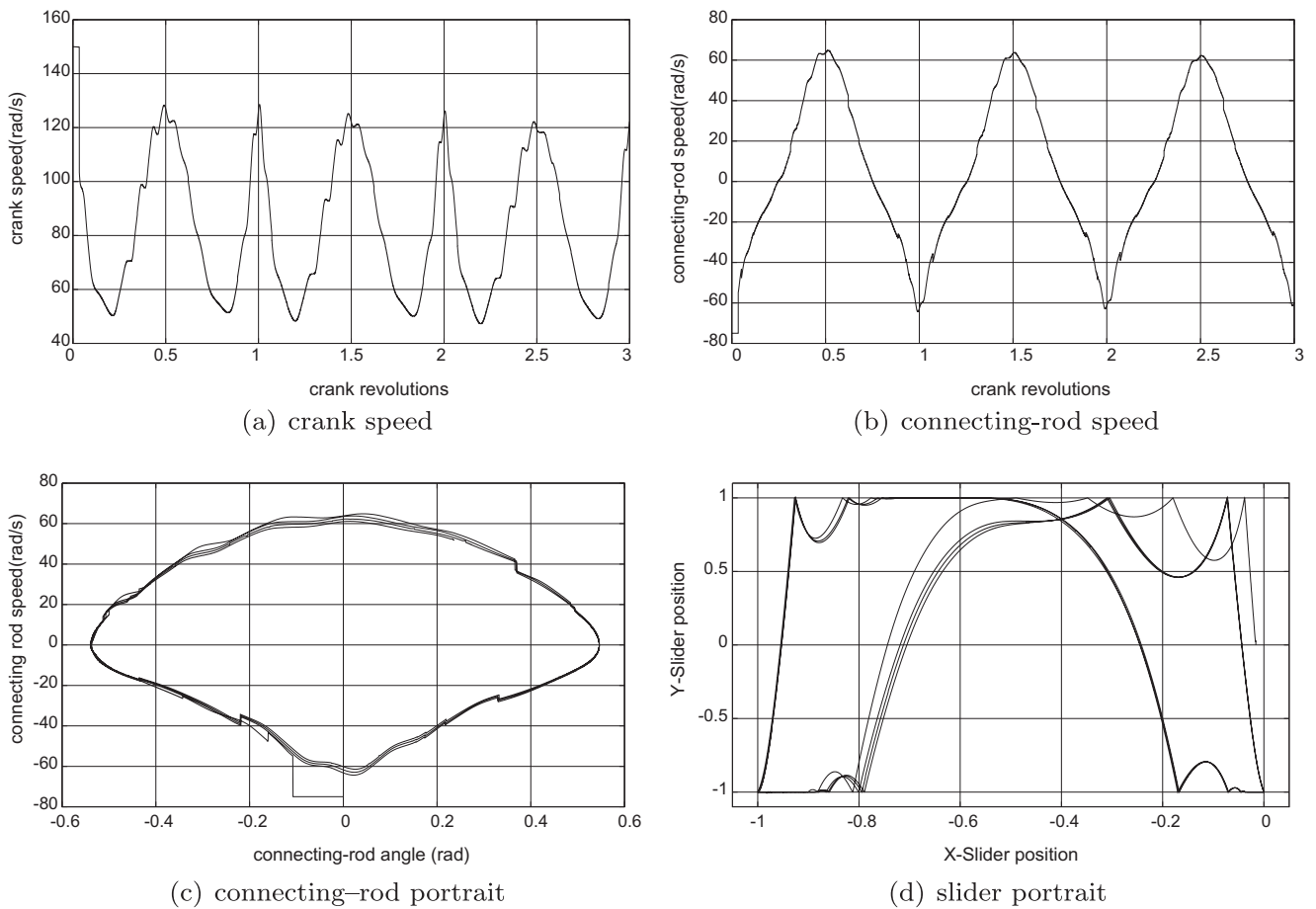


Fig. 28. Details of the motion of the slider crank with the combined projection time-stepping scheme for $h = 10^{-05}$ s and a play in the revolute joint $r = 5 \times 10^{-03}$ m.

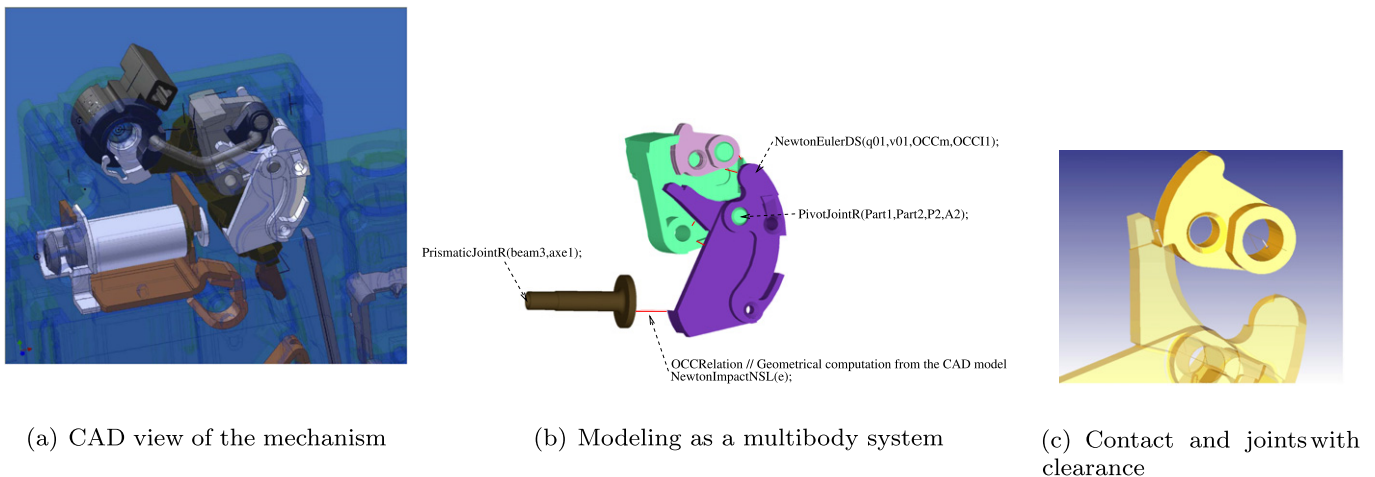


Fig. 29. C60 electrical circuit breaker mechanism. Courtesy of Schneider Electric.

we observe a complete change of the periodic motion just before the end of the second crank revolution. This reveals that the contact in the revolute joint is lost during the simulation mainly due to too large constraints violations. During the motion, the CAD library is not able to follow correctly the contact point and the contact detection failed because the geometries interpenetrate. This problem can be fixed with a smaller time-step, for instance $h = 10^{-07}$ s that limits the violation of constraints. In Fig. 27, the problem is solved with the same time-step $h = 10^{-05}$ s by using

the combined projection algorithm described in Algorithm 2. In Fig. 28, the simulation is performed with a one-order larger clearance in the revolute joint $r = 5 \times 10^{-03}$ m and shows larger oscillations around the nominal motion.

6.4. Electrical circuit breaker's mechanisms

In this final section, we give an insight of the usefulness of the proposed projected schemes for the virtual prototyping of

electrical circuit breakers designed by the company Schneider Electric. The C60 model that we considered here, is a domestic low voltage circuit breaker depicted on Fig. 29. The mechanism is only composed of seven moving bodies, but 12 contacts come into play when the breaker switches off. Furthermore, when the mechanism is in closed position, the equilibrium is guaranteed by means of Coulomb's friction in the contact of the two bodies described in Fig. 29(c). When the breaker opens the circuit, a lot of events (impacts, stick-slip transitions, ...) are observed in experimental setups. A rather complete description of its behavior and its nonsmooth modeling in 2D can be found in [1]. The study in 3D with clearances that is performed with the scheme described in Algorithm 2 allows us to accurately study the effect of the clearances in joints on the out-of-plane motion of the breaker. Furthermore, it helps to state on the stability and the robustness of the fundamental properties of the circuit breaker with respect to the size of the clearances. Such studies are not possible with standard event-driven schemes which have a lot of difficulties to deal with 3D frictional contacts and a bunch of events. Indeed, the presence of clearances in joints generates a lot of finite accumulation of impacts and numerous stick-slip transitions. Such studies are also difficult with standard event-capturing schemes for which the violation of constraints come into play with the characteristic lengths of the clearances.

7. Concluding remarks

In this paper, an efficient strategy is proposed to perform the time-discretization of nonsmooth multibody systems that satisfies in discrete time both the constraints at the position level and at the velocity level. This strategy consists in:

- a first *direct project scheme* which both satisfies in discrete time the position constraints and the velocity constraints, i.e., the impact law. This scheme based on the Moreau–Jean time-stepping scheme is a direct extension of Gear–Gupta–Leimkuhler (GGL) method [18] to unilateral constraints and impacts. The algorithm keeps the order of the standard Moreau–Jean scheme and the multiplier associated with the projection vanishes at the order $\mathcal{O}(h)$. With the decoupled approach, the implementation is straightforward and requires only slight modifications of the standard Moreau–Jean scheme. This direct projected scheme efficiently performs on most applications. Nevertheless, in the special case of the stabilization on the constraints after a finite accumulation of impacts, the direct application of the GGL technique yields chattering at contact.
- an improved *combined projection/activation scheme* has been proposed to circumvent this problem and to make robust the simulation with the respect to the activation strategy of constraints. We end up with an event-capturing time-stepping scheme which retains the most favorable properties of the direct scheme (order, simple implementation and efficiency, respect of position and velocity constraints) avoiding the artificial oscillations at contact of the relative velocity.

The efficiency and the robustness of the schemes have been shown on several academic examples and illustrated on an industrial application. The schemes are freely available in the open-source platform SICONOS with the examples developed in this article.

Further works must be done on the filtering of artificial high frequencies modes that occurs when a jump of velocity travels into a flexible structure discretized by finite elements. A first step has been done in [12] by adapting standard schemes for elastodynamics (HHT, α -schemes) that provides a targeted numerical damping. The proposed projected approaches could also be extended to the

schemes presented in [12]. The question of shock wave capturing methods in such applications has also to be studied in the light of recent work on time-integration techniques for shock wave propagation (see [41] and references therein).

Acknowledgments

This work has been supported by the French National Research Agency (ANR) through COSINUS program (project SALADYN ANR-08-COSI-014) <<http://saladyn.inria.gforge.fr/>>. The author is indebted to Olivier Bonnefon (INRIA) for the first implementation of the direct projected scheme on the slider–crank mechanism and the circuit breaker. Céline Acary-Robert is also acknowledged for her careful reading. Finally, Michel Abadie (Schneider Electric) is acknowledged for the industrial collaboration on circuit breakers.

References

- [1] M. Abadie, Dynamic simulation of rigid bodies: modelling of frictional contact, in: B. Brogliato (Ed.), Impacts in Mechanical Systems: Analysis and Modelling, Lecture Notes in Physics (LNP), vol. 551, 2000, pp. 61–144.
- [2] V. Acary, Toward higher order event-capturing schemes and adaptive time-step strategies for nonsmooth multibody systems. Research Report RR-7151, INRIA, 2009.
- [3] V. Acary, Higher order event capturing time-stepping schemes for nonsmooth multibody systems with unilateral constraints and impacts, Appl. Numer. Math. 62 (2012) 1259–1275.
- [4] V. Acary, B. Brogliato, Numerical Methods for Nonsmooth Dynamical Systems: Applications in Mechanics and Electronics, Lecture Notes in Applied and Computational Mechanics, vol. 35, Springer-Verlag, 2008.
- [5] V. Acary, F. Cadoux, C. Lemaréchal, J. Malick, A formulation of the linear discrete Coulomb friction problem via convex optimization, ZAMM – J. Appl. Math. Mech./Z. Angew. Math. Mech. 91 (2) (2011) 155–175.
- [6] V. Acary, F. Pèrignon, An introduction to Siconos. Technical Report TR-0340, INRIA, <http://hal.inria.fr/inria-00162911/en/>, 2007.
- [7] P. Ballard, The dynamics of discrete mechanical systems with perfect unilateral constraints, Arch. Ration. Mech. Anal. 154 (2000) 199–274.
- [8] P. Ballard, Bounded variations and measure theory on the line, Lectures notes of the second summer on Nonsmooth Dynamics held in Autrans (France), 2003.
- [9] O.A. Bauchau, A. Laulusa, Review of contemporary approaches for constraint enforcement in multibody systems, J. Comput. Nonlinear Dyn. 3 (1) (2008) 011005.
- [10] B. Brogliato, Nonsmooth Mechanics: Models, Dynamics and Control, second ed., Springer-Verlag, London, 1999.
- [11] N.J. Carpenter, R.L. Taylor, M.G. Katona, Lagrange constraints for transient finite element surface contact, Int. J. Numer. Methods Engrg. 38 (1991) 103–128.
- [12] Q.Z. Chen, V. Acary, G. Virlez, O. Brüls, A newmark-type integrator for flexible systems considering nonsmooth unilateral constraints, in: Peter Eberhard (Ed.), The Second Joint International Conference on Multibody System Dynamics – IMSD 2012, Stuttgart, Germany, March 2012.
- [13] G. De Saxcé, Z.-Q. Feng, New inequality and functional for contact with friction: the implicit standard material approach, Mech. Struct. Mach. 19 (1991) 301–325.
- [14] P. Deuffhard, R. Krause, S. Ertel, A contact-stabilized Newmark method for dynamical contact problems, Int. J. Numer. Methods Engrg. 73 (9) (2007) 1274–1290.
- [15] D. Doyen, A. Ern, S. Piperno, Time-integration schemes for the finite element dynamic Signorini problem, SIAM J. Sci. Comput. 33 (2011) 223–249.
- [16] R. Dzonou, M.D.P. Monteiro Marques, L. Paoli, A convergence result for a vibro-impact problem with a general inertia operator, Nonlinear Dyn. 58 (1–2) (2009) 361–384.
- [17] R. Flores, P. Leine, C. Glocker, Modeling and analysis of planar rigid multibody systems with translational clearance joints based on the non-smooth dynamics approach, Multibody Syst. Dyn. 23 (2010) 165–190.
- [18] C.W. Gear, B. Leimkuhler, G.K. Gupta, Automatic integration of Euler–Lagrange equations with constraints, J. Comput. Appl. Math. 12–13 (1985) 77–90.
- [19] F. Génot, B. Brogliato, New results on Painlevé paradoxes, Eur. J. Mech. A/Solids 18 (1999) 653–677.
- [20] H. Goldstein, Classical Mechanics, second ed., Addison-Wesley Pub. Co., 1980.
- [21] M. Géradin, A. Cardona, Flexible Multibody Dynamics: A finite element Approach, J. Wiley & Sons, New York, 2001.
- [22] E. Hairer, Ch. Lubich, G. Wanner, Geometric Numerical Integration. Structure-Preserving Algorithms for Ordinary Differential Equations, second ed., Springer, 2006.
- [23] T.J.R. Hughes, The Finite Element Method, Linear Static and Dynamic Finite Element Analysis, Prentice-Hall, New Jersey, 1987.

- [24] T.J.R. Hughes, R.L. Taylor, J.L. Sackman, A. Curnier, W. Kanoknukulchai, A finite element method for a class of contact-impact problems, *Comput. Methods Appl. Mech. Engrg.* 8 (1976) 249–276.
- [25] O. Janin, C.H. Lamarque, Comparison of several numerical methods for mechanical systems with impacts, *Int. J. Numer. Methods Engrg.* 51 (9) (2001) 1101–1132.
- [26] M. Jean, The non smooth contact dynamics method, in: J.A.C. Martins, A. Klarbring (Eds.), *Computational Modeling of Contact and Friction*, *Comput. Methods Appl. Mech. Engrg.* 177 (1999) 235–257 (special issue).
- [27] M. Jean, J.J. Moreau, Unilaterality and dry friction in the dynamics of rigid bodies collections, in: A. Curnier (Ed.), *Proc. of Contact Mech. Int. Symp.*, vol. 1, Presses Polytechniques et Universitaires Romandes, 1992, pp. 31–48.
- [28] F. Jourdan, P. Alart, M. Jean, A Gauss Seidel like algorithm to solve frictional contact problems, *Comput. Methods Appl. Mech. Engrg.* 155 (1) (1998) 31–47.
- [29] H.B. Khenous, P. Laborde, Y. Renard, On the discretization of contact problems in elastodynamics, in: Peter Wriggers et al. (Eds.), *Analysis and simulation of contact problems. Papers Based on the Presentation at the Fourth Contact Mechanics International Symposium (CMIS 2005)*, Loccum, Germany, July 4–6, 2005, *Lecture Notes in Applied and Computational Mechanics*, vol. 27, Springer, Berlin, 2006, pp. 31–38.
- [30] H.B. Khenous, P. Laborde, Y. Renard, Mass redistribution method for finite element contact problems in elastodynamics, *Eur. J. Mech. A Solids* 27 (5) (2008) 918–932.
- [31] T.A. Laursen, V. Chawla, Design of energy conserving algorithms for frictionless dynamic contact problems, *Int. J. Numer. Methods Engrg.* 40 (1997) 863–886.
- [32] T.A. Laursen, G.R. Love, Improved implicit integrators for transient impact problems – geometric admissibility within the conserving framework, *Int. J. Numer. Methods Engrg.* 53 (2002) 245–274.
- [33] T.A. Laursen, G.R. Love, Improved implicit integrators for transient impact problems – Dynamical frictional dissipation within an admissible conserving framework, *Comput. Methods Appl. Mech. Engrg.* 192 (2003) 2223–2248.
- [34] M.D.P. Monteiro Marques, *Differential Inclusions in Nonsmooth Mechanical Problems. Shocks and Dry Friction*, *Progress in Nonlinear Differential Equations and their Applications*, vol. 9, Birkhauser, Basel, 1993.
- [35] J.J. Moreau, Unilateral contact and dry friction in finite freedom dynamics, in: J.J. Moreau, Panagiotopoulos P.D. (Eds.), *Nonsmooth Mechanics and Applications*, CISM, Courses and Lectures, vol. 302, Springer-Verlag, Wien-New York, 1988, pp. 1–82.
- [36] J.J. Moreau, Numerical aspects of the sweeping process, in: J.A.C. Martins, A. Klarbring (Eds.), *Computational Modeling of Contact and Friction*, *Computer Methods in Applied Mechanics and Engineering* 177 (1999) 329–349 (special issue).
- [37] J.M. Ortega, W.C. Rheinboldt, *Iterative Solution of Nonlinear Equations in Several Variables*, *Classics in Applied Mathematics*, SIAM, 2000.
- [38] L. Paoli, An existence result for non-smooth vibro-impact problems, *J. Differ. Equat.* 211 (2005) 247–281.
- [39] L. Paoli, M. Schatzman, A numerical scheme for impact problems I: the one-dimensional case, *SIAM J. Numer. Anal.* 40 (2) (2002) 702–733.
- [40] L. Paoli, M. Schatzman, A numerical scheme for impact problems II: the multi-dimensional case, *SIAM J. Numer. Anal.* 40 (2) (2002) 734–768.
- [41] K.C. Park, S.J. Lim, H. Huh, A method for computation of discontinuous wave propagation in heterogeneous solids: basic algorithm description and application to one-dimensional problems, *Int. J. Numer. Methods Engrg.* 91 (6) (2012) 622–643.
- [42] F. Pfeiffer, C. Glocker, *Multibody Dynamics with Unilateral Contacts Non-linear Dynamics*, John Wiley & Sons, 1996.
- [43] PythonOCC. 3D CAD/CAE/PLM development framework for the Python programming language. <<http://www.pythonocc.org>>.
- [44] F. Radjaï, F. Dubois (Eds.), *Discrete-element modeling of granular materials*, ISTE, John Wiley & Sons, 2011.
- [45] R.T. Rockafellar, *Convex Analysis*, Princeton University Press, 1970.
- [46] M. Schatzman, A class of nonlinear differential equations of second order in time, *Nonlinear Anal. T.M.A* 2 (3) (1978) 355–373.
- [47] M. Schatzman, A hyperbolic problem of second order with unilateral constraints: the vibrating string with a concave obstacle, *J. Math. Anal. Appl.* 73 (1) (1980) 138–191.
- [48] M. Schatzman, Un problème hyperbolique du 2ème ordre avec contrainte unilatérale: La corde vibrante avec obstacle ponctuel, *J. Differ. Equat.* 36 (2) (1980) 295–334.
- [49] M. Schatzman, M. Bercovier, Numerical approximation of a wave equation with unilateral constraints, *Math. Comput.* 53 (187) (1989) 55–79.
- [50] T. Schindler, V. Acary, Timestepping schemes for nonsmooth dynamics based on discontinuous Galerkin methods: definition and outlook, *Mathematics and Computers in Simulation*, in press. <http://dx.doi.org/10.1016/j.matcom.2012.04.012>.
- [51] Siconos. A software for modeling and simulation of nonsmooth dynamical systems. <<http://siconos.gforge.inria.fr>>.
- [52] D. Stewart, Convergence of a time-stepping scheme for rigid-body dynamics and resolution of Painlevé's problem, *Arch. Ration. Mech. Anal.* 145 (1998) 215–260.
- [53] D. Stewart, Rigid body dynamics with friction and impact, *SIAM Rev.* 42 (1) (2000) 3–39.
- [54] C. Studer, *Numerics of Unilateral Contacts and Friction. Modeling and Numerical Time Integration in Non-Smooth Dynamics*, *Lecture Notes in Applied and Computational Mechanics*, Springer-Verlag, 2009.
- [55] C. Studer, R.I. Leine, Ch. Glocker, Step size adjustment and extrapolation for time stepping schemes in non-smooth dynamics, *Int. J. Numer. Methods Engrg.* 76 (11) (2008) 1747–1781.
- [56] T.A. Laursen, *Computational Contact and Impact Mechanics – Fundamentals of Modeling Interfacial Phenomena in Nonlinear Finite Element Analysis*, Springer-Verlag, 2003.
- [57] Open CASCADE Technology. <<http://www.opencascade.org>>.
- [58] P. Wriggers, *Computational Contact Mechanics*, second ed., Springer-Verlag, 2006. Originally published by John Wiley & Sons Ltd., 2002.